

Semiclassical simulations of multidimensional Raman echoes

Shaul Mukamel, Andrei Piryatinski, and Vladimir Chernyak

Department of Chemistry, University of Rochester, Rochester, New York 14627-0216

(Received 4 September 1998; accepted 14 October 1998)

A high-temperature and a weak-nonlinear (low-temperature) semiclassical expansion are developed for computing two-dimensional vibrational Raman spectroscopies, and applied to an exactly solvable Brownian-oscillator model. The origin of photon echoes is discussed using phase-space-wave-packets. Impulsive and semi-impulsive echoes are shown to satisfy different phase-matching conditions, and are generated in different directions. © 1999 American Institute of Physics. [S0021-9606(99)51003-9]

I. INTRODUCTION

In coherent time-resolved multidimensional Raman spectroscopy, a molecular system is excited by a train of N pairs of nonoverlapping electronically off-resonant short pulses.¹⁻³ The superposition of vibrational states prepared by these pulses is then detected by the scattering of a final probe pulse (Fig. 1). The dimensionality (D) of these techniques is given by the number of time intervals between pulses. Coherent Raman scattering (CRS) is the lowest (1D) technique which provides information about vibrational frequencies and relaxation rates.⁴⁻⁸ 2D and 3D techniques provide much more detailed information regarding intermolecular and intramolecular structure and dynamics in liquids, proteins, polymers, and glasses with complex vibrational structure.⁹⁻¹²

3D coherent Raman scattering, which is similar to stimulated photon echo⁹ was first proposed in Ref. 1 and measured in Refs. 13,14. The lower order (2D) Raman technique, proposed by Tanimura and Mukamel^{2,15} is now the subject of intense experimental¹⁶⁻²¹ and theoretical^{15,22-27,18} activity. Contributions of the anharmonicity of vibrational modes and the nonlinear dependence of the electronic polarizability to the optical response have been investigated. New resonances at combinations of single oscillator resonant frequencies (cross peaks) have been predicted and observed.^{16,22,23,28} In addition, these techniques can distinguish between homogeneous and inhomogeneous spectral line broadening mechanisms. For inhomogeneous broadening, the signal has a photon echo form²⁴ and carries information about relaxation time scales as well as vibrational mode frequencies. Suppression of the photon echo due to the vibrational mode coupling via polarization has been demonstrated by numerical simulations.²⁷

Extracting structural and dynamical information from multidimensional signals requires the computation of nonlinear response functions,³ taking into account the combined effect of anharmonicities, nonlinear dependence of the polarizability on nuclear coordinates, and the quantum character of nuclear motions. In off-resonant Raman spectroscopies, coupling with the radiation field is given by the effective Hamiltonian²⁹

$$H_{\text{int}}(t) = -\mathcal{E}^2(t)\alpha(\mathbf{Q}), \quad (1.1) \quad \text{with}$$

where $\alpha(\mathbf{Q})$ is the electronic polarizability which depends on the vibrational coordinates (\mathbf{Q}). In 2D spectroscopy the radiation field is given by a sum of two nonoverlapping pulse pairs centered at times τ_1 and τ_2 (Fig. 1),

$$\mathcal{E}(t) = \sum_{j=1}^2 \mathcal{E}_j(t - \tau_j). \quad (1.2)$$

The signal is generated by the scattering of a probe field denoted $\mathcal{E}_p(t - \tau_p)$. The polarization (and the signal field) is proportional to the square of the field of each of the two driving pulses and to the probe field, and is altogether fifth order in the field

$$P^{(5)}(t) = \int_{-\infty}^{\infty} d\tau'_1 \int_{-\infty}^{\infty} d\tau'_2 R^{(5)}(t; \tau'_2, \tau'_1) \times \mathcal{E}_2^2(\tau'_2 - \tau_2) \mathcal{E}_1^2(\tau'_1 - \tau_1) \mathcal{E}_p(t - \tau_p). \quad (1.3)$$

The fifth order response function $R^{(5)}(t, \tau_2, \tau_1)$ is given by a combination of three-point correlation functions of the polarizability α

$$R^{(5)}(t; \tau_2, \tau_1) = \left(\frac{i}{\hbar}\right)^2 \langle \alpha_+(t) \alpha_-(\tau_2) \alpha_-(\tau_1) \rangle, \quad (1.4)$$

where $\alpha_+ \equiv (1/2)(\alpha_L + \alpha_R)$, and $\alpha_- \equiv \alpha_L - \alpha_R$; α_L (α_R) is the electronic polarization operator acting on the density superoperator from the left (right). The time evolution of $\alpha(t)$ is given by the free molecular Hamiltonian (without the radiation field). This expression contains four terms representing all possible combinations of ‘‘left’’ and ‘‘right’’ actions of the three polarization operators.³⁰ Each term corresponds to a distinct Liouville-space path, and can be represented by a double-sided Feynman diagram Fig. 2.³ The various correlation functions interfere, giving rise to many interesting effects such as new resonances.

For completeness we also present the third order (1D) response,

$$P^{(3)}(t) = \int_{-\infty}^{\infty} d\tau'_1 R^{(3)}(t; \tau'_1) \mathcal{E}_1^2(\tau'_1 - \tau_1) \mathcal{E}_p(t - \tau_p), \quad (1.5)$$

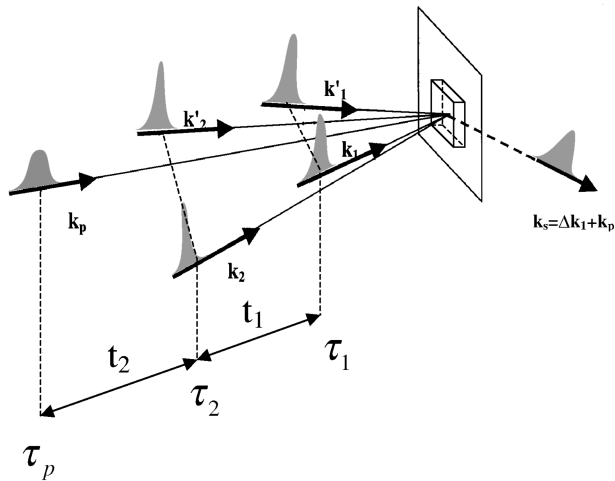


FIG. 1. Geometry and time-ordering of the incoming pulse sequence in fifth order 2D spectroscopy. The first pair of pulses comes at τ_1 and the second at τ_2 . t_1 and t_2 are the time intervals. $\Delta \mathbf{k}_1 \equiv \mathbf{k}_1 - \mathbf{k}'_1$, $\Delta \mathbf{k}_2 \equiv \mathbf{k}_2 - \mathbf{k}'_2$. Only one of the nine possible signals pulses (in the direction $\mathbf{k}_s = \Delta \mathbf{k}_1 + \mathbf{k}_p$) is shown.

$$R^{(3)}(t; \tau_1) = \frac{i}{\hbar} \langle \alpha_+(t) \alpha_-(\tau_1) \rangle. \quad (1.6)$$

In this article we investigate the application of semiclassical techniques towards the molecular dynamics simulation of the nonlinear response function [Eq. (1.4)]. Formally, these techniques employ an expansion in powers of \hbar .³¹⁻³³ The $1/\hbar^2$ prefactor in Eq. (1.4) suggests an apparent divergence as $\hbar \rightarrow 0$. However, when the four correlation functions are combined, the $1/\hbar^2$ factor is canceled for small \hbar , and one obtains a finite classical response, independent of \hbar . Semiclassical simulations should not, therefore, aim at the individual correlation functions $\langle \alpha(\tau_1) \alpha(\tau_2) \alpha(\tau_3) \rangle$ which do not have an obvious classical limit, but focus instead on the entire response function (which is a specific combination of four correlation functions), that must have a classical limit.

In our earlier studies we have identified two different semiclassical expansions which differ in the choice of the zero order (classical) limit. The first starts with the standard high temperature (HT) limit. When $k_B T$ is large compared with the vibrational frequencies we have³⁴

$$R_{\text{HT}}^{(3)}(t; \tau) = \beta \frac{d}{d\tau_1} \langle \alpha(t) \alpha(\tau_1) \rangle_c, \quad (1.7)$$

$$R_{\text{HT}}^{(5)}(t; \tau_2, \tau_1) = \beta^2 \frac{d^2}{d\tau_2 d\tau_1} \langle \alpha(t) \alpha(\tau_2) \alpha(\tau_1) \rangle_c - \beta \frac{d}{d\tau_1} \sum_{ijk} \langle \epsilon_{ij} M_{jk}(\tau_2, \tau_1) \alpha(t) \times \alpha'_i(\tau_2) \alpha'_k(\tau_1) \rangle_c. \quad (1.8)$$

Here $\beta = (k_B T)^{-1}$, $\langle \dots \rangle_c$ denote classical correlation function $\alpha'_i \equiv \partial \alpha / \partial x_j$ and $x_1 \equiv p$, $x_2 \equiv q$, and $\epsilon_{ii} = 0$, $\epsilon_{1,2} = -\epsilon_{2,1} = 1$. $M_{jk}(\tau_2, \tau_1)$ for $i, j = 1, 2$ is the stability matrix defined as the derivative of a small deviation $\delta x_k(\tau_1)$ at time τ_1 with respect to a small deviation $\delta x_j(\tau_2)$ at time τ_2 , and

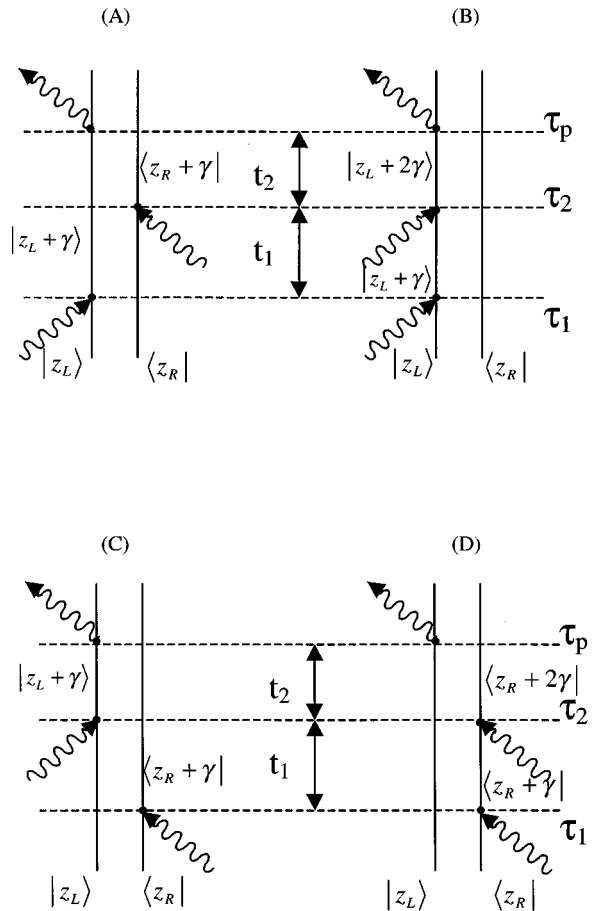


FIG. 2. Double-sided Feynman diagrams representing the four Liouville space pathways contributing to the fifth-order response of the model harmonic system coupled to the radiation field via electronic polarizability with exponential dependence on nuclear coordinates [Eq. (2.3)]. The coherent state representation ($|z_L\rangle$, and $|z_R\rangle$) is adopted (Ref. 15), $\gamma = Q_0^{-1} \sqrt{\hbar/(2M\Omega)}$ [see Eq. (5.1)]. Each diagram corresponds to the propagation of the phase-space wave packet $\rho_\alpha^W(P, Q)$ given by Eq. (2.11) with (A) $j=0, k=1$, (B) $j=0, k=0$, (C) $j=1, k=0$, and (D) $j=1, k=1$.

relates small deviations δx_j to δx_k at different times. For a single degree of freedom (q, p) this matrix satisfies the equation:

$$\frac{\partial}{\partial \tau_2} M_{jk}(\tau_2, \tau_1) = \begin{pmatrix} -\partial^2 H / \partial q^2 & -\partial^2 H / \partial q \partial p \\ \partial^2 H / \partial p \partial q & \partial^2 H / \partial p^2 \end{pmatrix} M_{jk}(\tau_2, \tau_1) \quad (1.9)$$

with the boundary conditions $M_{jk}(\tau_1, \tau_1) = \delta_{jk}$.

The first term in Eq. (1.8), related to the three-point correlation function of the polarizability, is a straightforward generalization of the fluctuation-dissipation relation [Eq. (1.7)]. It can be computed by sampling classical trajectories with thermal equilibrium initial conditions. Unlike the first term in Eq. (1.8) which contains no interference (merely averaging over the initial density matrix), the second term shows interesting classical interference, as suggested by the presence of the stability matrix; for each initial phase-space point we need to launch two trajectories with very close initial conditions. The nonlinear response is obtained by adding the contributions of these trajectories and letting them interfere.

Intramolecular and intermolecular vibrational motions typically span a broad frequency range, (both lower and higher than $k_B T/\hbar$). In liquid water, for example, the spectral density covers the 0–1000 cm^{-1} range, whereas $k_B T$ at room temperature is $\sim 200 \text{ cm}^{-1}$. The high-temperature approximation cannot be used to describe high frequency motions. Fortunately, a classical simulation of the optical response may still be possible, even though the system itself is quantum mechanical.²⁸ This is based on the observation that the optical response of a linearly driven harmonic oscillator is always linear and classical, regardless of temperature. The two sources of nonlinearities (anharmonicities and nonlinear dependence of α on \mathbf{Q}) are therefore responsible for the nonlinear response as well as for its nonclassical nature. This suggests that a semiclassical expansion for both sources of optical nonlinearity may be possible, as long as these nonlinearities are sufficiently weak. We denote this the weak nonlinearity (WN) expansion. The lowest order contribution to the response is temperature-independent; the temperature shows up only in higher-order terms. Explicit expression for the WN are given in Ref. 28 and discussed in Appendix C.

The HT expansion is formally obtained by expanding $R^{(5)}$ in powers of \hbar , keeping T fixed, whereas in the WN expansion we keep the thermal frequency $\omega_T \equiv k_B T/\hbar$ fixed. The latter thus contains an implicit dependence on \hbar (through ω_T) even as $\hbar \rightarrow 0$. For both expansions, in the classical limit (to zero order in \hbar) the signal can be calculated by solving the classical equations of motion. The polarization (and the classical response) is given by $\alpha(\tau) = \alpha(\mathbf{Q}(\tau))$, where $\mathbf{Q}(\tau)$ evolve using classical trajectories. In the HT expansion the initial conditions should sample the actual phase space equilibrium distribution. The WN expansion only requires a single trajectory with initial zero coordinate and momentum. This trajectory represents the evolution of a wave packet induced by coupling to the radiation field.

The Planck constant constitutes a convenient bookkeeping device for computing high order (quantum) corrections for both expansions. The Wigner–Kirkwood semiclassical expansion provides quantum corrections to a desired power in \hbar , using the Wigner (phase-space) representation.³⁵

The article is organized as follows: in Sec. II we derive an exact quantum mechanical expression for the optical response of a nonlinearly driven Brownian oscillator, and represent it using phase-space wave packets. The fifth order response function is represented in terms of a superposition of Gaussian wave packets which retain their forms under the system-field interaction.^{36,37} The exact quantum response function $R^{(5)}$ is computed for a simple model of a single underdamped Brownian oscillator coupled to the radiation field via electronic polarizability which has exponential dependence on the nuclear coordinates. The classical high temperature (HT) and weak nonlinearity (WN) limits of the response function as well as for the phase-space wave packets are given in Sec. III. By varying two dimensionless parameters we show how the exact expression for $R^{(5)}$ reduces to the HT and WN limiting cases. In Sec. IV we compute the response of an underdamped Brownian oscillator, which shows multiple echoes generated by the excitation of high order coherences. The range of applicability of the HT and

WN approximations is explored. We also model the HT optical response for a harmonic system with low-frequency vibrations with comparable central frequency and homogeneous width. Using the WN expansion we compare two spectroscopic regimes; impulsive (pulses are shorter than nuclear dynamics and relaxation time scales) and semi-impulsive (pulses are long compared to the time scale of nuclear dynamics but short compared to the inhomogeneous dephasing time). The classical WN picture of the photon echo based on the phase-space wave packet representation is given in Sec. V. The phase-space WN dynamics associated with 2D Raman echoes is consistent with the classical picture commonly used in NMR spectroscopy.^{38,39} Adopting the WN approximation, we represent in Sec. VI the signal from a multi-mode anharmonic system in the frequency domain, and demonstrate the semiclassical origin of the resonances at combinations of vibrational frequencies (cross peaks). Our results are finally summarized in Sec. VII.

II. THE FIFTH ORDER RESPONSE OF A BROWNIAN OSCILLATOR

We consider a molecule with a single primary Raman-active harmonic vibrational degree of freedom Q , coupled to the optical field via the electronic polarizability $\alpha(Q)$, and interacting with a large number of harmonic (bath) coordinates which induce relaxation and dephasing. The Hamiltonian has a form:

$$H = H_m + H_{\text{int}}(t) + H_B. \quad (2.1)$$

The molecular Hamiltonian representing the primary Raman active mode is given by

$$H_m = \frac{P^2}{2M} + \frac{M\Omega^2 Q^2}{2}, \quad (2.2)$$

where P , Q , Ω , and M are the momentum, coordinate frequency, and mass of the primary mode, and H_{int} [Eq. (1.1)] represents its coupling to the driving field. We assume exponential dependence of the electronic polarizability on the nuclear coordinate

$$\hat{\alpha}(Q) = \alpha_0 \exp(Q/Q_0). \quad (2.3)$$

H_B represents the bath Hamiltonian and its coupling to the primary vibrational mode. For clarity we shall first consider an isolated vibration and set $H_B = 0$, H_B will be specified later.

In the impulsive limit, where pulse durations are much shorter than the delay between pulses and the nuclear dynamics time scales, the time-resolved heterodyne signal $S^{(5)}(t_2, t_1)$ depends on the two time delays t_1 and t_2 between pulses (Fig. 1) and is proportional to the fifth-order response function

$$S(t_2, t_1) = R^{(5)}(t_2 + t_1; t_1, 0). \quad (2.4)$$

For our model, the molecular dynamics underlying $R^{(5)}$ can be represented using Gaussian wave packets for the density matrix in the Wigner representation.^{3,37} At thermal equilibrium we have

$$\bar{\rho}(P, Q) = \frac{\Omega}{2\pi\sigma} \exp\left(-\frac{P^2}{4M\sigma} - \frac{M\Omega^2 Q^2}{4\sigma}\right) \quad (2.5)$$

with the variance $\sigma \equiv (\hbar\Omega/2)/\coth(\hbar\Omega/2k_B T)$. Equation (1.4) depends on the superoperator $\alpha_- = \alpha_L - \alpha_R = \alpha_0[\exp(Q_L/Q_0) - \exp(Q_R/Q_0)]$ which in the Wigner representation assumes the form

$$\alpha_- = \alpha_0 \exp\left(\frac{Q}{Q_0} + \frac{i\hbar}{2Q_0} \frac{\partial}{\partial P}\right) - \alpha_0 \exp\left(\frac{Q}{Q_0} - \frac{i\hbar}{2Q_0} \frac{\partial}{\partial P}\right). \quad (2.6)$$

The action of the two terms (corresponding to α_L or α_R) in the right-hand side of Eq. (2.6) on a Gaussian wave packet can be viewed as evolution in imaginary time with respect to an operator linear in Q and $\partial/\partial P$. This evolution preserves the Gaussian form of the wave packet; its variances (i.e., the set of the second moments) do not change whereas the position of its center (the first moments) are time dependent. Since the α_- operator is a linear combination of α_L and α_R (Eq. (2.6)), the density matrix $\alpha_- \bar{\rho}$ produced at $\tau=0$ as a result of the first interaction with the driving field is a superposition of two Gaussian wave packets whose centers subsequently rotate in the (P, Q) phase space with frequency Ω . A straightforward calculation yields the following form of the wave packet during the first time interval, assuming that the first interaction comes at $\tau=0$,

$$\begin{aligned} \rho^{(1)}(P, Q; \tau) = & \sum_{j=0,1} (-1)^j \frac{\alpha_0}{i\hbar} \exp\left[\frac{\bar{Q}_j(0)}{2Q_0}\right] \\ & \times \frac{\Omega}{2\pi\sigma} \exp\left\{-\frac{[P - \bar{P}_j(\tau)]^2}{4M\sigma} \right. \\ & \left. - \frac{M\Omega^2 [Q - \bar{Q}_j(\tau)]^2}{4\sigma}\right\}, \quad (2.7) \end{aligned}$$

where $j=0,1$ stand for L (left) and R (right), respectively, and

$$\bar{Q}_j(\tau) = \bar{Q}_j(0) \cos(\Omega\tau) + \frac{\bar{P}_j(0)}{M\Omega} \sin(\Omega\tau), \quad (2.8)$$

$$\bar{P}_j(\tau) = M\dot{\bar{Q}}_j(\tau) \quad (2.9)$$

describe the classical phase-space trajectories of the wave packet centers with the initial conditions⁴⁰

$$\bar{Q}_j(0) = \frac{2\sigma}{M\Omega^2 Q_0}; \quad \bar{P}_j(0) = (-1)^{j+1} \frac{i\hbar}{2Q_0}. \quad (2.10)$$

The second interaction with the driving field at $\tau=t_1$ produces a pair of Gaussian wave packets out of each of the two given by Eq. (2.7). The density matrix during the second time interval is thus given by a superposition of four wave packets,

$$\rho^{(2)}(P, Q; \tau) = \sum_{jk=0,1} \rho_{jk}^{(2)}(P, Q; \tau) \quad (2.11)$$

with

$$\begin{aligned} \rho_{jk}^{(2)}(P, Q; \tau) = & (-1)^{k+j} \frac{\alpha_0^2}{(i\hbar)^2} \exp\left[\frac{\bar{Q}(0) + \bar{Q}_j(t_1)}{Q_0}\right], \\ & \times \frac{\Omega}{2\pi\sigma} \exp\left[-\frac{(P - \bar{P}_j(\tau) - \bar{P}_k(\tau - t_1))^2}{4M\sigma} \right. \\ & \left. - \frac{M\Omega^2 (Q - \bar{Q}_j(\tau) - \bar{Q}_k(\tau - t_1))^2}{4\sigma}\right], \quad (2.12) \end{aligned}$$

where $\bar{Q}_j(\tau)$ and $\bar{P}_j(\tau)$ are given by Eqs. (2.8) and (2.9). The four terms in Eq. (2.12) correspond to four Liouville space pathways represented by the Feynman diagrams for the nonlinear response and given in Fig. 2. The subscript j determines the type (left or right action) of the first interaction with the driving field, whereas k is related to the second interaction.

Using these wave packets, the impulsive signal is given by

$$\begin{aligned} S^{(5)}(t_2, t_1) = & \int dP \int dQ \alpha(Q) \rho^{(2)}(P, Q; t_2 + t_1) \\ = & \alpha_0 \sum_{kj=0,1} \int dP \int dQ \\ & \times \exp\left(\frac{Q}{Q_0}\right) \rho_{kj}^{(2)}(P, Q; t_2 + t_1). \quad (2.13) \end{aligned}$$

Substitution of Eqs. (2.11) and Eq. (2.12) into Eq. (2.13) yields the final expression for $R^{(5)}$

$$\begin{aligned} R^{(5)}(t_2 + t_1, t_1; 0) = & -\frac{2\alpha_0^3}{\hbar^2} A \exp\left[\frac{\hbar}{Q_0^2} f(t_2 + t_1, t_1; 0)\right] \\ & \times \sin\left[\frac{\hbar}{2Q_0^2} (C(t_2 + t_1) + C(t_1))\right] \sin\left[\frac{\hbar}{2Q_0^2} C(t_2)\right], \quad (2.14) \end{aligned}$$

where

$$f(t_2 + t_1, t_1; 0) \equiv C^{(+)}(t_2 + t_1) + C^{(+)}(t_2) + C^{(+)}(t_1), \quad (2.15)$$

$$A \equiv \exp\left[\frac{3\hbar}{2Q_0^2} C^{(+)}(0)\right].$$

Here $C(t) \equiv (i\hbar)^{-1} \langle Q_+(t) Q_-(0) \rangle$ and $C^{(+)}(t) \equiv \hbar^{-1} \langle Q_+(t) Q_+(0) \rangle$ are the Liouville space correlation functions of the oscillator coordinate operator. These have the form

$$C(t) = -\theta(t) \frac{4}{M\Omega} \sin(\Omega t), \quad (2.16)$$

$$C^{(+)}(t) = \frac{2}{M\Omega} \coth\left(\frac{\hbar\Omega}{2k_B T}\right) \cos(\Omega t).$$

The third order response is similarly given by

$$R^{(3)}(t, \tau_1) = \frac{2\alpha_0^2}{\hbar} \exp\left[\frac{\hbar}{Q_0^2} C^{(+)}(0)\right] \times \exp\left[\frac{\hbar}{Q_0^2} C^{(+)}(t - \tau_1)\right] \times \sin\left[\frac{\hbar}{2Q_0^2} C(t - \tau_1)\right]. \quad (2.17)$$

Equation (2.17) may be obtained directly from Eqs. (1.6) using the second order cumulant expansion. The more lengthy wave packet approach given here allows us to trace the semiclassical origin of the response.

To include the coupling to a bath, we adopt the Brownian oscillator model by adding a harmonic bath linearly coupled to the primary mode.⁴¹ The system-bath dynamics is now determined by the Hamiltonian [Eq. (2.1)] with

$$H_B = \sum_{\alpha} \left[\frac{p_{\alpha}^2}{2m_{\alpha}} + \frac{m_{\alpha}\omega_{\alpha}^2}{2} \left(q_{\alpha} - \frac{c_{\alpha}}{m_{\alpha}\omega_{\alpha}} Q \right)^2 \right], \quad (2.18)$$

where $p_{\alpha}, q_{\alpha}, m_{\alpha}$, and ω_{α} are the momentum, coordinate mass and vibrational frequency of the α bath oscillator.

The optical response can again be found by following the dynamics of the Gaussian wave packets in the complete (system plus bath) phase space, since the system-bath Hamiltonian H_B is harmonic in the full phase space $\{P, Q, p_{\alpha}, q_{\alpha}\}$. This is a straightforward generalization of the single mode case. The response functions retain their form [(Eqs. (2.14), (2.15) and (2.17)]. However the correlation functions $C(t)$ and $C^{+}(t)$ are now given by

$$C(t) = -2\theta(t) \int_{-\infty}^{\infty} \frac{d\omega}{2\pi} C(\omega) \sin(\omega t), \quad (2.19)$$

$$C^{+}(t) \equiv \int_{-\infty}^{\infty} \frac{d\omega}{2\pi} C(\omega) \coth\left(\frac{\hbar\omega}{2kT}\right) \cos(\omega t), \quad (2.20)$$

with the spectral density

$$C(\omega) = \frac{1}{M} \frac{4\omega\gamma(\omega)}{(\Omega^2 + \omega\Sigma(\omega) - \omega^2)^2 + 4\omega^2\gamma^2(\omega)}. \quad (2.21)$$

$\gamma(\Delta)$ is the imaginary (real) parts of a self-energy operator representing relaxation (level shift),

$$\gamma(\omega) = \pi \sum_{\alpha} c_{\alpha}^2 [\delta(\omega - \omega_{\alpha}) + \delta(\omega + \omega_{\alpha})], \quad (2.22)$$

$$\Sigma(\omega) = -\frac{1}{\pi} PP \int_{-\infty}^{\infty} d\omega' \frac{\gamma(\omega')}{\omega' - \omega}.$$

Equations (2.14), (2.15), and (2.17), together with (2.19)-(2.21) constitute exact expressions for the response functions of a single Brownian oscillator whose polarizability α [Eq. (2.3)] is exponential in the primary coordinate. In the next section we compare these results with the HT and WN approximations for the optical response and the underlying wave packets.

III. CLASSICAL LIMITS FOR THE RESPONSE AND WAVE PACKETS

The WN response functions are obtained by expanding Eqs. (2.14) and (2.17) in powers of \hbar , holding ω_T fixed. In this case, $C^{(+)}(t)$ is independent on \hbar . The expansion of sines in Eq. (2.14) starts with $\sim \hbar^2$ terms, and the classical approximation is obtained by retaining only the first term in the expansion, and setting the factor A and the exponent in Eq. (2.14) to unity. This yields

$$R_{WN}^{(3)}(t, \tau_1) = \frac{\alpha_0^2}{Q_0^2} C(t - \tau_1), \quad (3.1)$$

and

$$R_{WN}^{(5)}(t_2 + t_1, t_1; 0) = \frac{\alpha_0^3}{Q_0^4} [C(t_2)C(t_2 + t_1) + C(t_2)C(t_1)]. \quad (3.2)$$

The HT approximation is obtained by expanding $R^{(3)}$ and $R^{(5)}$ in powers of \hbar holding T fixed. The sines in Eqs. (2.14) and (2.17) are expanded in the same way as for the WN approximation. Expanding A and $f(t_1 + t_2, t_1; 0)$ to lowest order in \hbar we set $\coth(\hbar\omega/2kT) \approx 2kT/\hbar\omega$ in Eq. (2.20), and obtain

$$R_{HT}^{(3)}(t; \tau) = \exp\left[\frac{2k_B T}{Q_0^2} \bar{C}(0)\right] \times \exp\left[\frac{2k_B T}{Q_0^2} \bar{C}(t - \tau_1)\right] R_{WN}^{(3)}(t, \tau_1), \quad (3.3)$$

and

$$R_{HT}^{(5)}(t_2 + t_1, t_1; 0) = \bar{A} \exp\left[\frac{2kT}{Q_0^2} \bar{f}(t_2 + t_1, t_1; 0)\right] \times R_{WN}^{(5)}(t_2 + t_1, t_1; 0). \quad (3.4)$$

\bar{f} is given by Eq. (2.15) by simply replacing $C^{(+)}(t)$ with $\bar{C}(t)$

$$\bar{C}(t) \equiv \int_{-\infty}^{\infty} \frac{d\omega}{2\pi} \frac{C(\omega)}{\omega} \cos(\omega t), \quad (3.5)$$

and

$$\bar{A} \equiv \exp\left[\frac{3kT}{Q_0^2} \bar{C}(0)\right]. \quad (3.6)$$

Here we have derived the HT and WN approximations by expanding the exact solution. For more general models where the exact solution is not available, it is still possible to obtain these approximations directly, order by order. For the WN, this procedure is described in Ref. 28, whereas for the HT it is given in Ref. 34.

The significance of both approximations can be clarified by following the corresponding wave packet dynamics. In the solution given in Sec. II we start with a single Gaussian wave packet $\bar{\rho}(P, Q)$, and each interaction with the driving field doubles the number of wave packets; we have a super-

position of two Gaussians during t_1 and a superposition of four during t_2 . In contrast, in both classical limits the system can be represented by a single Gaussian wave packet at all times. In the HT limit the wave packets evolve according to classical trajectories, i.e., the wave packet $\rho(P, Q; \tau)$ at time τ at the phase-space point (P,Q) is given by the value $\rho(P_0, Q_0; 0)$ of the wave packet at $\tau=0$. P_0 and Q_0 are the initial conditions for the classical trajectory which reaches (P,Q) at time τ . For a harmonic system, this prescription yields a single Gaussian wave packet at all times. In particular for the single-mode model without a bath introduced in Sec. II we have during the t_2 time interval

$$\rho_{\text{HT}}^{(2)}(P, Q; \tau) = \frac{\alpha_0^2}{(2Q_0)^2} [\sin(\Omega t_1) + \sin(\Omega \tau)] \times \sin(\Omega(\tau - t_1)) \exp\left[\frac{\bar{Q}(0) + \bar{Q}(t_1)}{Q_0}\right] \times \frac{\Omega}{2\pi k_B T} \exp\left[-\frac{(P - \bar{P}(\tau) - \bar{P}(\tau - t_1))^2}{4Mk_B T} - \frac{M\Omega^2(Q - \bar{Q}(\tau) - \bar{Q}(\tau - t_1))^2}{4k_B T}\right], \quad (3.7)$$

with the center coordinates

$$\begin{aligned} \bar{Q}(0) &= \frac{2k_B T}{M\Omega^2 Q_0}, \\ \bar{Q}(\tau) &= \bar{Q}(0) \cos(\Omega \tau), \\ \bar{P}(\tau) &= M\dot{\bar{Q}}(\tau). \end{aligned} \quad (3.8)$$

The WN dynamics is also given by a single Gaussian wave packet but for a different reason. For a linearly driven harmonic system the wave packet remains Gaussian at all times. Adding both types of nonlinearities [anharmonicity and nonlinearity in the electronic polarizability $\alpha(Q)$] leads to deviation from the Gaussian form. However, to lowest order in the nonlinearities (which corresponds to the zeroth order in \hbar for ω_T fixed) we can neglect the variation of the second moments and the nonlinearities only affect the trajectory through the first moments. This yields

$$\rho(P, Q; \tau) = \frac{\Omega}{2\pi\sigma} \exp\left\{-\frac{[P - \bar{P}(\tau)]^2}{4M\sigma} - \frac{M\Omega^2[Q - \bar{Q}(\tau)]^2}{4\sigma}\right\} \quad (3.9)$$

with $\sigma \equiv (\hbar\Omega/2)/\coth(\hbar\Omega/2k_B T)$. $\bar{P}(\tau)$, $\bar{Q}(\tau)$ is the classical trajectory in the phase space with the initial conditions $\bar{P}(0) = \bar{Q}(0) = 0$.³⁷ The response functions are obtained by expanding the trajectory in powers of the driving field

$$\begin{aligned} \bar{P}(\tau) &= \bar{P}^{(1)}(\tau) + \bar{P}^{(2)}(\tau) + \dots, \\ \bar{Q}(\tau) &= \bar{Q}^{(1)}(\tau) + \bar{Q}^{(2)}(\tau) + \dots \end{aligned} \quad (3.10)$$

$\bar{P}^{(j)}(\tau)$, $\bar{Q}^{(j)}(\tau)$ can be computed by the substitution of Eq. (3.10) into the classical equations of motion of the externally

driven system and solving them order by order in the field. Substituting the wave packets [Eqs. (3.7) and (3.9)] in to Eq. (2.13) yields the response functions $R^{(5)}$ in the form of Eqs. (3.2) and (3.4), respectively.

Although the reason why we only have a single Gaussian is different for the HT and WN, it can be rationalized using the same argument. Different phase-space trajectories determined by Eqs. (2.8) and (2.9) and related to different Gaussian wave packets coincide if we set the initial momentum $\bar{P}_j(0)$ [Eq. (2.10)] to zero. The magnitude of $\bar{P}_j(0)$ is proportional to \hbar and is independent of temperature. This means that for both HT and WN, semiclassical expansions of all the Gaussian wave packets in the superposition merge to a single Gaussian in the $\hbar \rightarrow 0$ limit. The exact quantum density matrix of our model is given by a superposition of four Gaussian wave packets each associated with a distinct Liouville space pathway. In both semiclassical expansions the width of the equilibrium wave packet along the momentum direction is larger than the separation between the four trajectories determined by $\bar{P}_j(0)$, and these four wave packets can be approximated by a single one. In the HT limit when both anharmonicity and nonlinearity are taken into account, the wave packet strongly deviates from a Gaussian form whereas in the WN the deviations are assumed small and an expansion in these deviations is made.

In the next section we present numerical calculations of impulsive 2D signals, and test the regions of validity of both semiclassical expansions.

IV. MULTIPLE FIFTH-ORDER ECHOES

In this section we study the role of homogeneous and inhomogeneous broadening as probed by impulsive 2D spectroscopy. We use the Brownian oscillator model [Eq. (2.21)] with a ω -independent damping term γ (Ohmic dissipation) which immediately implies $\Sigma = 0$.

We first consider a high-frequency weakly-damped mode with $\gamma \ll \Omega$. The correlation functions $C(t)$ and $C^{(+)} \times(t)$ are then given by

$$\begin{aligned} C(t) &= -\theta(t) \frac{4}{M\Omega} \sin(\Omega t) e^{-\gamma t}, \\ C^{(+)}(t) &= \frac{2}{M\Omega} \coth\left(\frac{\hbar\Omega}{2k_B T}\right) \cos(\Omega t) e^{-\gamma|t|}. \end{aligned} \quad (4.1)$$

Substituting Eq. (4.1) into Eq. (2.14) and making use of Eq. (2.4) we obtain

$$\begin{aligned} S^{(5)}(t_2, t_1) &= -\frac{8}{(g\hbar)^2} (\tilde{\alpha}^{(1)})^2 \tilde{\alpha}^{(2)} A \\ &\times \exp\left[g\hbar \coth\left(\frac{g\hbar}{2g_T}\right) \tilde{f}(t_2, t_1)\right] \\ &\times \sin\{g\hbar(\sin(\Omega(t_2 + t_1)) e^{-\gamma(t_2 + t_1)} \\ &+ \sin(\Omega t_1) e^{-\gamma t_1})\} \sin\{g\hbar \sin(\Omega t_2) e^{-\gamma t_2}\}, \end{aligned} \quad (4.2)$$

where

$$\begin{aligned} \tilde{f}(t_2, t_1) &\equiv \cos(\Omega(t_2 + t_1))e^{-\gamma(t_2+t_1)} \\ &+ \cos(\Omega t_1)e^{-\gamma t_1} + \cos(\Omega t_2)e^{-\gamma t_2}, \\ A &\equiv \exp\left[\frac{3}{2}g_h \coth\left(\frac{g_h}{2g_T}\right)\right]. \end{aligned} \tag{4.3}$$

Here $\tilde{\alpha}^{(1)} \equiv \alpha_0 / (\sqrt{M\Omega Q_0})$ and $\alpha^{(2)} \equiv \alpha_0^2 / (M\Omega Q_0)$. To analyze the range of applicability of both expansions, we first introduce the quantum length $Q_h: \hbar\Omega \equiv (1/2)M\Omega^2 Q_h^2$, and the thermal length $Q_T: kT \equiv (1/2)M\Omega^2 Q_T^2$ related to the zero-point and thermal energies, respectively. By dividing these lengths by the nonlinearity length scale Q_0 we obtain the dimensionless parameters $g_h \equiv (Q_h/Q_0)^2$ and $g_T \equiv (Q_T/Q_0)^2$. The WN expansion holds when $g_h, g_T \ll 1$. Expanding Eq. (4.2) to lowest order in these parameters gives

$$\begin{aligned} S_{\text{WN}}^{(5)} &= -8(\tilde{\alpha}^{(1)})^2 \tilde{\alpha}^{(2)} \\ &\times (\sin(\Omega(t_1 + t_2))\sin(\Omega t_2)e^{-\gamma(t_1+2t_2)} \\ &+ \sin(\Omega t_1)\sin(\Omega t_2)e^{-\gamma(t_1+t_2)}). \end{aligned} \tag{4.4}$$

The HT expansion requires $Q_h \ll Q_T$. Taking the limit $g_h \rightarrow 0$, Eq. (4.2) yields for a fixed value of g_T ,

$$S_{\text{HT}}^{(5)} \equiv \exp(3g_T) \exp[2g_T \tilde{f}(t_1, t_2)] S_{\text{WN}}^{(5)}. \tag{4.5}$$

Making two-dimensional Fourier transformation of Eq. (4.2), the exact optical signal $S(t_2, t_1) \equiv R^{(5)}(t_2 + t_1; t_1, 0)$ assumes the form

$$\begin{aligned} S(t_2, t_1; \Omega) &= \sum_{n,m=-\infty}^{\infty} e^{-i\Omega(mt_2 - nt_1)} F_{nm}(e^{-\gamma t_2}, e^{-\gamma t_1}; g_h, g_T). \end{aligned} \tag{4.6}$$

The two-dimensional Fourier coefficients F_{nm} in Eq. (4.6) have the form

$$\begin{aligned} F_{nm} &= -\frac{8}{(g_h)^2} (\tilde{\alpha}^{(1)})^2 \tilde{\alpha}^{(2)} \int_{-\pi}^{\pi} \frac{d\theta_1}{2\pi} \int_{\pi}^{\pi} \frac{d\theta_2}{2\pi} \\ &\times \exp\left[g_h \coth\left(\frac{g_h}{2g_T}\right) \tilde{f}(\theta_2, \theta_1)\right] \\ &\times \sin\{g_h(\sin(\theta_2 + \theta_1)e^{-\gamma(t_2+t_1)} \\ &+ \sin(\theta_1)e^{-\gamma t_1})\} \sin\{g_h \sin(\theta_2)e^{-\gamma t_2}\} e^{i(m\theta_2 - n\theta_1)}, \end{aligned} \tag{4.7}$$

where $\tilde{f}(\theta_2, \theta_1) \equiv \cos(\theta_2 + \theta_1)e^{-\gamma(t_2+t_1)} + \cos(\theta_1)e^{-\gamma t_1} + \cos(\theta_2)e^{-\gamma t_2}$. The magnitudes of F_{nm} which vary on the homogeneous relaxation time-scale γ^{-1} and depend parametrically on g_h , and g_T determine the relative amplitudes of the signal components. In the HT approximation, the expansion coefficients adopt the form

$$\begin{aligned} F_{nm}^{\text{HT}} &= -4(\tilde{\alpha}^{(1)})^2 \tilde{\alpha}^{(2)} \sum_{j,k=\pm 1} jk [K_{n+j, m+k} e^{-\gamma(t_1+t_2)} \\ &+ K_{n+j, m+k-1} e^{-\gamma(t_1+2t_2)}], \end{aligned} \tag{4.8}$$

with the auxiliary function K_{nm}

$$\begin{aligned} K_{nm} &= \sum_{l=-\infty}^{\infty} (-1)^{m+n+l} I_{l+n}(g_T e^{-\gamma t_1}) I_{l-m}(g_T e^{-\gamma t_2}) \\ &\times I_l(g_T e^{-\gamma(t_1+t_2)}), \end{aligned} \tag{4.9}$$

where $I_l(x)$ ($l=0,1,2,\dots$) are the modified Bessel functions. Taking the $g_T \rightarrow 0$ limit in Eq. (4.8) and making use of the fact that only $I_0(0)=1$ does not vanish for zero argument, we find that only four coefficients survive in the WN expansion of Eq. (4.6)

$$\begin{aligned} F_{nm}^{\text{WN}} &= 8mn(\tilde{\alpha}^{(1)})^2 \tilde{\alpha}^{(2)} \exp[-\gamma(t_1+t_2)], \\ F_{n;m\pm 1}^{\text{WN}} &= 8mn(\tilde{\alpha}^{(1)})^2 \tilde{\alpha}^{(2)} \exp[-\gamma(t_1+2t_2)], \end{aligned} \tag{4.10}$$

where $m, n = \pm 1$.

We next assume that the oscillator frequency has an inhomogeneous Gaussian distribution,

$$W(\Omega) = \frac{1}{\sqrt{2\pi}\Delta} \exp\left[-\frac{(\Omega - \Omega_0)^2}{2\Delta^2}\right], \tag{4.11}$$

where the inhomogeneous width Δ satisfies

$$\hbar \gamma \ll \hbar \Delta \ll \hbar \Omega_0, kT. \tag{4.12}$$

When the oscillator is weakly-damped and the linewidth is dominated by inhomogeneous dephasing, the 2D signal shows an echo.³ Convoluting Eq. (4.6) with the Gaussian distribution function $W(\Omega)$ [Eq. (4.11)] we obtain for the signal

$$S(t_2, t_1) \equiv \int d\Omega W(\Omega) S(t_2, t_1; \Omega), \tag{4.13}$$

$$\begin{aligned} S(t_2, t_1) &= \sum_m e^{-im\Omega_0 t_2} \sum_n \exp\left[-\frac{(m\Delta)^2}{2} \left(t_2 - \frac{nt_1}{m}\right)^2\right] \\ &\times e^{in\Omega_0 t_1} F_{nm}(e^{-\gamma t_2}, e^{-\gamma t_1}; g_h, g_T). \end{aligned} \tag{4.14}$$

This signal shows multiple echoes at all possible time combinations $t_2 = (n/m)t_1$, $m, n = 1, 2, 3, \dots$. The relative magnitudes of the echo peaks and the echo decay due to homogeneous broadening are determined by F_{nm} . The echo decay reflects the homogeneous dephasing time scale $T_2 = \gamma^{-1}$. For a fixed t_1 , oscillations of the echo signal with t_2 are independent of n and have the period $(m\Omega_0)^{-1}$. The width of the echo signal at a fixed t_1 is also independent of n and reflects the inhomogeneous dephasing time scale $T_1 = (m\Delta)^{-1}$. The multiple echoes presented by Eq. (4.14) originate from high order vibrational coherences created by the exponential electronic polarizability $\alpha(Q)$ which contains all orders in Q/Q_0 . Computer simulations of HT multiple echoes for different values of g_T were presented in Ref. 23.

We next compare the exact, HT and the WN approximations to Eq. (4.14) using numerical simulations. We discuss the results using the (g_h, g_T) -phase diagram shown in Fig. 3. The WN holds when only the first term which is unity in the expansion of the exponential prefactor in Eq. (4.2) can be retained as well as g_h is small enough to retain only the first term in the expansion of the sines. To neglect the contribution of the second term in the expansion of the exponential

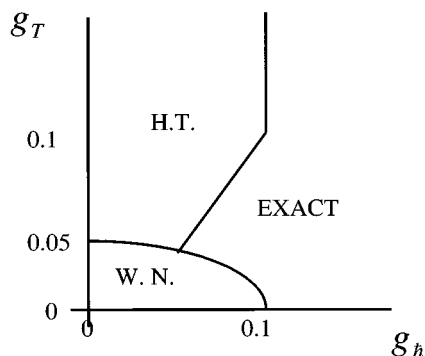


FIG. 3. (g_T, g_h) -phase diagram showing range of applicability of the high temperature (HT) and the weak nonlinearity (WN) approximations. The region where both classical approximation fail is denoted "exact."

prefactor we require it to be less or equal to 0.1, which amounts to $g_T \leq g_h / 2 \operatorname{arcoth}(0.1/g_h)$. The region where this inequality holds is denoted in the plot as WN. The HT holds for small values of $g_h < 0.1$, provided the argument of the exponential prefactor in Eq. (4.2) is approximated as $g_h \coth(g_h/(2g_T)) \sim 2g_T$ which is satisfied provided $g_T \geq g_h$. This region is marked HT. The WN and HT regions may overlap. Transition through the common boundary from HT to WN leads to the decrease of g_T in the argument of the exponential prefactor in Eq. (4.5), making it small enough to approximate the exponent by unity. In this case Eqs. (4.4) and (4.5) coincide. Transition from the WN to HT regions increases the value of g_T , and higher order terms in the expansion of the exponent in Eq. (4.5) should be included. We refer to these high temperature corrections as classical.

The WN echo, shown in Fig. 4(a) whose magnitude is determined by the functions $F_{11}(g_T \rightarrow 0)$ and $F_{-1-1}(g_T \rightarrow 0)$ [Eq. (4.10)], appears only in the $t_2 = t_1$ direction. The first classical corrections to the WN signal at a small value of g_T [$F_{\pm 1 \pm 2}(g_T)$ and $F_{\pm 2 \pm 1}(g_T)$, Eq. (4.8)], show up according to Eq. (4.14) as additional echoes at $t_2 = t_1/2, 2t_1$. We present the HT signal at the point $g_T = 0.05$ ($g_h = 0$) which lies on the boundary between the WN and HT regions of the phase diagram in Fig. 4(b). Additional echoes associated with classical corrections to the WN signal are clearly seen in this plot. As g_T is increased the number of echoes increases as well,²³ and the WN approximation fails. The exact signal computed for $g_h = 0$ irrespective of g_T coincides with signals in the classical approximations.

The corrections to the WN on the boundary which does not overlap with the HT region on the phase diagram are due to the expansion of the exponential prefactor and sines in Eq. (4.2) in powers of g_h . A general procedure for computing these "quantum" corrections was developed in Ref. 28. According to Eq. (4.14), quantum corrections result in additional echoes. In the same way, additional echoes appear when g_h exceeds the value where the high temperature approximation holds. To demonstrate this we present in Fig. 4(c) the exact signal computed at $g_h = 0.5$ and $g_T = 0.05$. Comparing it with the HT (b) and WN (a) signals we observe additional echoes at $t_2 = 3t_1, t_1/3$. Both classical approximations fail in this case.

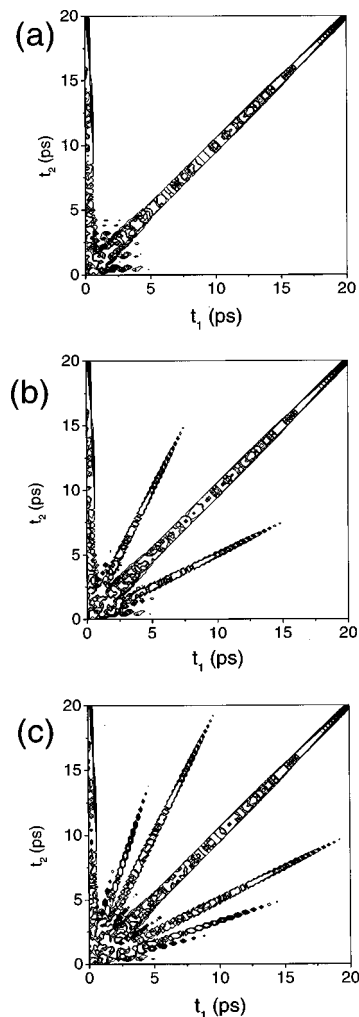


FIG. 4. Absolute square of the echo signals $|S^{(5)}(t_1, t_2)|^2$ computed for an underdamped harmonic system exponentially coupled to the radiation field with central frequency $\Omega = 508 \text{ cm}^{-1}$, homogeneous width $\gamma = 1 \text{ cm}^{-1}$, and inhomogeneous width $\Delta = 30 \text{ cm}^{-1}$. (a) WN approximation, $g_h = g_T = 0$. Only one echo is seen in the direction $t_1 = t_2$. (b) HT approximation $g_h = 0$, $g_T = 0.05$, additional echoes in the $t_1/t_2 = 1/2, 2$ directions show that the WN approximation is not valid for this set of parameters. (c) Exact quantum response $g_h = 0.5$, $g_T = 0.05$, additional echoes in the $t_1/t_2 = 1/3, 1/2, 2, 3$ directions demonstrate that neither the WN nor the HT hold for this set of parameters. In all plots the signal stretched along t_2 axis, $t_1 = 0$ is due to the vibrational state population excitation.

We next turn to low frequency intermolecular modes. We consider a weakly overdamped $\Omega_0 \lesssim \gamma$ oscillator with $\Omega_0 = 20 \text{ cm}^{-1}$ and $\gamma = 30 \text{ cm}^{-1}$, and the following form for the inhomogeneous distribution:

$$W(\Omega) \propto \mathcal{N} \Omega^4 \exp \left[- \frac{(\Omega - \Omega_0)^2}{2\Delta^2} \right]. \quad (4.15)$$

The Ω^4 prefactor provides a low-frequency cutoff which is required to get physically acceptable signals.

We set $g_T = 0.05$ and varied the inhomogeneous width Δ between 10 cm^{-1} and 60 cm^{-1} . We have computed the high-temperature response function [Eq. (2.14)]. The time domain spectral densities Eqs. (2.19) and (2.20) and the signal averaged over the distribution given by Eq. (4.15) were calculated numerically. The results are presented in Fig. 5.

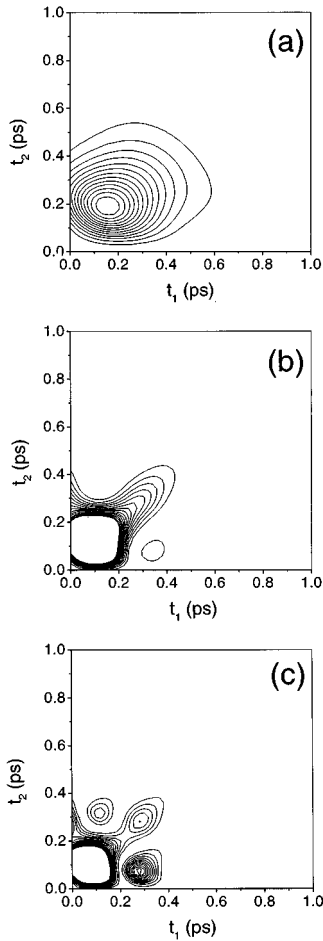


FIG. 5. Absolute square of the signal $|S^{(5)}(t_1, t_2)|^2$ computed in the HT approximation for the model low frequency harmonic system exponentially coupled to the radiation field with central frequency $\Omega = 60 \text{ cm}^{-1}$, homogeneous width $\gamma = 30 \text{ cm}^{-1}$, and $g_T = 0.05$. Inhomogeneous width (a) $\Delta = 10 \text{ cm}^{-1}$, no echo, (b) $\Delta = 30 \text{ cm}^{-1}$ weak echo stretched in $t_1 = t_2$ direction, and (c) $\Delta = 60 \text{ cm}^{-1}$ signal oscillations are clearly seen.

Panel (a) shows a contour plot of the signal for $\Delta = 10 \text{ cm}^{-1}$. No echo is observed in this case. Increasing Δ to 30 cm^{-1} and 60 cm^{-1} [panels (b),(c)] leads to the generation of a weak echo at $t_1 = t_2$. Panel (c) further shows oscillations of the echo with a period determined by the frequency spread in the interval $(\Omega_0, \Omega_0 + \Delta/2)$.

V. THE CLASSICAL ORIGIN OF PHOTON ECHOES

In the previous section we have compared the exact 2D signals with the HT and WN approximations. For strong inhomogeneous broadening, the signals show echoes in both the quantum and classical regime. This implies that the photon echo is not necessarily a quantum phenomenon, as might be inferred from the standard calculation for a two-level system.^{38,39} In this section we first present a simple classical picture of WN photon echoes using phase-space wave packets in the impulsive regime where pulse durations τ_p are short compared to the vibrational periods $\tau_p \ll \Omega^{-1}$. We then discuss another interesting ‘‘semi-impulsive’’ case where this condition does not hold.

As shown in Sec. III, WN signals are determined by the classical phase-space trajectory of the Gaussian wave packet center. For clarity, we consider a single inhomogeneously broadened mode and neglect the bath, setting $\gamma = 0$. We further introduce the complex variable $z(\tau)$ which maps the phase space onto the complex plane

$$z(\tau) = \frac{1}{(2M\Omega)^{1/2}} [M\Omega\bar{Q}(\tau) + i\bar{P}(\tau)] \quad (5.1)$$

and constitutes the classical analog of the oscillator annihilation operator. The signal $S^{(5)}$ is determined by Eq. (2.13). To obtain the WN approximation we expand the exponential factor in this expression to first order in Q/Q_0 . Integration over P and Q using the wave packet [Eqs. (3.9) and (3.10)] shows that the response function is proportional to $\bar{Q}^{(2)}(\tau)$. In terms of our complex coordinate it is given by the real part of the second-order term $z^{(2)}$ of the expansion of $z(t)$ in powers of the driving field,

$$S_h = \sqrt{2}\tilde{\alpha}^{(1)} \text{Re}[z^{(2)}(\tau)]E_p(\tau)E_h^*(\tau), \quad (5.2)$$

where $\tilde{\alpha}^{(1)} = \alpha_0 / \sqrt{M\Omega}Q_0$, and \mathcal{E}_p and \mathcal{E}_h are the envelopes of the probe and heterodyne fields. The phase-matching condition for the signal which determines its propagation direction is discussed in Appendix A. For impulsive excitation, the second-order solution of the classical equation of motion (following the interaction with the two pulse-pairs) can be represented in the matrix form

$$Z(t_2 + t_1) = G_\Omega(t_2)X_2G_\Omega(t_1)Z_1, \quad (5.3)$$

where

$$Z(t) \equiv \begin{pmatrix} z^{(2)}(t) \\ z^{(2)*}(t) \end{pmatrix}, \quad (5.4)$$

$$Z_1 \equiv \frac{i}{2\sqrt{2}}\tilde{\alpha}^{(1)}F_1(1 + \cos(\Delta\mathbf{k}_1 \cdot \mathbf{r})) \begin{pmatrix} 1 \\ -1 \end{pmatrix}, \quad (5.5)$$

$$X_2 \equiv \frac{i}{4}\tilde{\alpha}^{(2)}F_2(1 + \cos(\Delta\mathbf{k}_2 \cdot \mathbf{r})) \begin{pmatrix} 1 & 1 \\ -1 & -1 \end{pmatrix}, \quad (5.6)$$

$$G_\Omega(t) \equiv \begin{pmatrix} e^{-i\Omega t} & 0 \\ 0 & e^{i\Omega t} \end{pmatrix}, \quad (5.7)$$

where $\Delta\mathbf{k}_j$, F_j ($j = 1, 2$) are defined by Eqs. (A5) and (A9). Equation (5.3) describes the dynamics of the system in terms of the complex variables $z(t)$ and (its complex conjugate) $z^*(t)$ in the complex plane (q, ip). Initially, the system is at thermal equilibrium and $z = z^* = 0$. The first pulse produces a state Z_1 [Eq. (5.5)]. In this state, the vector $z(0)$ [$z^*(0)$] [the upper (lower) component of (5.5)] is oriented along the positive (negative) direction of the imaginary axis ip . The Green’s function $G_\Omega(t_1)$ propagates this state during the first time interval between the pulses, rotating $z(0)$ and $z^*(0)$ in opposite directions with the angular frequency Ω . For an ensemble of systems with a broad frequency distribution $W(\Omega)$, the t_1 -propagation dephases the coherence, destroying the signal. The action of the second pulse is described by the matrix X_2 [Eq. (5.6)]. The diagonal elements only change the absolute values and phases (by $\pi/2$) of $z(t_1)$ and $z^*(t_1)$;

the subsequent t_2 evolution $G_\Omega(t_2)$ only increases the dephasing and the optical signal vanishes on the inhomogeneous broadening time scale. In contrast, the off-diagonal elements of X_2 not only change the magnitudes and phases of the $z(t_1)$ and $z^*(t_1)$ but also switch these vectors such that their t_2 -propagation is represented by rotation with the same frequency Ω but in the reverse direction compared with the t_1 -rotation. This gives rise to rephasing which ultimately leads to the photon echo.³⁸

Computing $\text{Re } z^{(2)}(t_1+t_2)$ with the help of Eqs. (5.3)–(5.7) and inserting the result into Eq. (5.2) one obtains for the heterodyne signal

$$S_{ih}^{(5)}(t_1, t_2; \Omega) = \frac{1}{8} (\tilde{\alpha}^{(1)})^2 \tilde{\alpha}^{(2)} F_1 F_2 F_p a_i(\mathbf{k}_s) \times \sin(\Omega t_1) \sin(\Omega t_2), \quad (5.8)$$

where $a_i(\mathbf{k}_s)$ is the angular distribution factor given by Eq. (A13) which confines the signal to the nine directions given by $\mathbf{k}_s = \mathbf{k}_p + m\Delta\mathbf{k}_1 + n\Delta\mathbf{k}_2$, $m, n = 0, \pm 1$. Averaging over the Gaussian distribution Eq. (4.11) yields the echo signal given in Eq. (A12).

So far all our calculations assumed impulsive excitation with $\tau_p \ll \Omega^{-1}$, (τ_p being the pulse duration). Another interesting regime is when the pulses are long compared to the vibrational periods but short compared to the inhomogeneous dephasing time scale Δ^{-1} , $\Omega^{-1} \ll \tau_p \ll \Delta^{-1}$. Expressions for semi-impulsive WN echoes are derived in Appendix B starting with Eq. (3.2). This is done in the rotating frame by introducing a new variable $w(t)$: $z(t) = w(t) \exp(-i\Omega_0 t)$. Ω_0 is the center frequency of the distribution function $W(\Omega_0)$ given by Eq. (4.11). In terms of $w(t)$ and $w^*(t)$ the second order solution of the classical equation of motion can be recast in the following matrix form:

$$W(t_2+t_1) = G_{\Omega-\Omega_0}(t_2) Y_2 G_{\Omega-\Omega_0}(t_1) W_1, \quad (5.9)$$

with

$$W(t) \equiv \begin{pmatrix} w^{(2)}(t) \\ w^{(2)*}(t) \end{pmatrix}, \quad (5.10)$$

$$W_1 \equiv \frac{i}{4\sqrt{2}} \tilde{\alpha}^{(1)} \begin{pmatrix} \mathcal{F}_1 e^{i\Delta\mathbf{k}_1 \mathbf{r}} \\ -\mathcal{F}_1^* e^{-i\Delta\mathbf{k}_1 \mathbf{r}} \end{pmatrix}, \quad (5.11)$$

$$Y_2 \equiv \frac{i}{8} \tilde{\alpha}^{(2)} \begin{pmatrix} \mathcal{F}_2^* e^{-i\Delta\mathbf{k}_2 \mathbf{r}} & \mathcal{F}_2 e^{i\Delta\mathbf{k}_2 \mathbf{r}} \\ -\mathcal{F}_2^* e^{-i\Delta\mathbf{k}_2 \mathbf{r}} & -\mathcal{F}_2 e^{i\Delta\mathbf{k}_2 \mathbf{r}} \end{pmatrix}, \quad (5.12)$$

where $\mathcal{F}_j, j=1,2$ are given by Eq. (B7) and the Green's function $G_{\Omega-\Omega_0}(t)$ is given by Eq. (5.7). The rotating wave approximation (RWA) has been employed in the derivation of Eq. (5.12); we only retain those elements in W_1 and Y_2 which do not oscillate with the optical frequency Ω . The discussion of the dynamics of the system which interacts with semi-impulsive pulses in terms of $w(t)$ and $w^*(t)$ is similar to that of the impulsive case in terms of $z(t)$ and $z^*(t)$. The heterodyne signal, derived using Eqs. (5.2), (5.9)–(5.12), has the form

$$S_{s_{ih}}^{(5)}(t_1, t_2; \Omega) = \frac{(\alpha^{(1)})^2 \alpha^{(2)}}{128(M\Omega)^2} \{ (2\pi)^3 \times \delta^{(3)}(\mathbf{k}_s - \mathbf{k}_p - \Delta\mathbf{k}_1 + \Delta\mathbf{k}_2) \times \text{Re}[\mathcal{F}_1 \mathcal{F}_2^* \mathcal{F}_p e^{-i(\Omega-\Omega_0)(t_1+t_2)}] + (2\pi)^3 \delta^{(3)}(\mathbf{k}_s - \mathbf{k}_p + \Delta\mathbf{k}_1 - \Delta\mathbf{k}_2) \times \text{Re}[\mathcal{F}_1^* \mathcal{F}_2 \mathcal{F}_p e^{-i(\Omega-\Omega_0)(t_2-t_1)}] \}. \quad (5.13)$$

Equation (5.13) shows two components of the signal propagating in the directions $\mathbf{k}_s = \mathbf{k}_p + \Delta\mathbf{k}_1 - \Delta\mathbf{k}_2$ ($\mathbf{k}_s = \mathbf{k}_p - \Delta\mathbf{k}_1 + \Delta\mathbf{k}_2$) determined by the diagonal (off-diagonal) elements of the matrix Y_2 in Eq. (5.9). The first signal vanishes on the inhomogeneous time scale whereas the second generates an echo. Averaging Eq. (5.13) over the Gaussian distribution $W(\Omega_0)$ [Eq. (4.11)] we obtain Eq. (B8) for the semi-impulsive signal.

The WN provides a clear picture for impulsive and semi-impulsive echoes. The semi-impulsive regime is intermediate between the pure impulsive and the CW (frequency domain) coherent 2D Raman scattering. Semi-impulsive pulses have a narrow bandwidth which allows a selective excitation of specific vibrations. The RWA which applies in this case leads to the generation of a signal in a single spatial direction. In contrast, impulsive excitation cannot discriminate between various propagation wave vectors, and the echo appears in all possible directions.

The effect of damping has been neglected in our wave packets Eqs. (2.7), (2.12), (3.7), and (A12). Since the center of the Gaussian wave packet obeys classical equations of motion, a friction force can be introduced. This force leads to a spiral motion of the wave packet center towards the origin.^{42,43} The relaxation in the Brownian oscillator model represents vibrational relaxation (T_1) and does not include pure vibrational dephasing (T_2). The latter requires an anharmonic system-bath coupling of the form Q^2q . Pure dephasing can then be treated perturbatively. 2D Raman spectroscopy can probe both the T_1 and T_2 homogeneous relaxation time scales.^{23,44} The signal stretched along the t_2 axis ($t_1=0$) in all panels of Fig. 4, is associated with the vibrational population excitation and should decay on T_1 time scale,⁴⁴ whereas the echo signal decays on the dephasing (T_2) time scale.

VI. SEMICLASSICAL ORIGIN OF CROSS PEAKS

The fifth-order response function of multi-mode vibrational systems carries information about intermode coupling through the electronic polarizability $\alpha(\mathbf{Q})$ and anharmonicity $V(\mathbf{Q})$. Anharmonicity neglected in previous section can be readily taken in the WN approximation. In Appendix C we present the multi-mode underdamped Brownian oscillator Hamiltonian Eq. (C1) used in Ref. 28. For this model, anharmonicities [Eq. (C2)] yield an additional contribution to the echo single which shifts the phase of its oscillations.²³ This is the case since the leading WN term does not affect the energy levels of the harmonic oscillator and they still form a harmonic ladder. As the anharmonicity is increased further, the level structure deviates from a simple harmonic ladder,

leading to dephasing and to the eventual disappearance of the echo. Suppression of the echo due to anharmonicities can be investigated in the HT limit using semiclassical simulations.

Cross correlations between modes are best displayed in the frequency domain

$$S(\omega_2, \omega_1) = \int_0^\infty dt_1 \int_0^\infty dt_2 e^{i\omega_1 t_1 + i\omega_2 t_2} R^{(5)}(t_2 + t_1; t_1; 0) \quad (6.1)$$

as the Fourier transform of the response function $R^{(5)}$ with respect to the time intervals. Intermode couplings give new resonances on combinations of vibrational frequencies (cross peaks). As shown in Appendix C, the WN signal has three contributions. The first term contributing to the total signal $S_1(\omega_2, \omega_1)$ [Eq. (C6)] shows (ω_1, ω_2) -resonances at the vibrational frequencies $(\pm\Omega_n, \pm\Omega_n)$ and $(\mp\Omega_n, \pm\Omega_n)$. The second term $S_2(\omega_2, \omega_1)$ [Eq. (C7)] shows cross peaks $(\pm\Omega_n, \pm(\Omega_n + \Omega_m))$, $(\pm\Omega_n, \pm(\Omega_m - \Omega_n))$, $(n \neq m)$ arising from nonlinear intermode coupling via off-diagonal elements of polarizability $\tilde{\alpha}_{nm}^{(2)}$ ($n \neq m$) as well as overtones and zero-frequency resonances associated with diagonal elements of $\tilde{\alpha}_{nn}^{(2)}$. The anharmonicity enters through the third component $S_3(\omega_2, \omega_1)$ [Eq. (C8)] which has the same resonances as $S_1(\omega_2, \omega_1)$ and $S_2(\omega_2, \omega_1)$ but their amplitudes are different. The cross peaks in this case are due to the anharmonic intermode coupling via off-diagonal elements of $\tilde{V}^{(3)}$. The 2D Raman spectra of two coupled weakly anharmonic oscillators are presented in Fig. 6. Panel (A) displays the contribution to the total signal given by the first term [Eq. (C6)] with the resonances on the vibrational frequencies only. Panel (B) shows the signal associated with the second term [Eq. (C7)] which consists of cross peaks 5–8 and 5'–8' due to intermode coupling via the polarizability components $\tilde{\alpha}_{12}^{(2)}$ and $\tilde{\alpha}_{21}^{(2)}$. Panel (C) presents the cross peaks 5–8 and 5'–8' associated with the anharmonicity coupling via $\tilde{V}_{112}^{(3)}$, $\tilde{V}_{121}^{(3)}$, $\tilde{V}_{211}^{(3)}$, $\tilde{V}_{122}^{(3)}$, $\tilde{V}_{212}^{(3)}$, $\tilde{V}_{221}^{(3)}$. The total signal displayed in panel (D) shows all the resonances of panels (A)–(C). Cross peaks have been observed experimentally in mixtures of liquids.¹⁶ The semiclassical response function given here allows us to compute these peaks in complex systems by solving classical equations of motion for vibrational coordinates.

VII. SUMMARY

In this article we have compared two different semiclassical expansions of the fifth-order off-resonant response function. We have analyzed their range of applicability using an exactly solvable model of a single-mode Brownian oscillator coupled to the radiation field via electronic polarizability which depends exponentially on nuclear coordinates. The exact quantum expression for the response function [Eq. (4.2)] reduces to the HT [Eq. (4.5)] and WN [Eq. (4.4)] limits by varying the dimensionless parameters g_h and g_T , as shown in the phase-diagram (Fig. 3). The underdamped Brownian oscillator shows multiple-echoes associated with vibrational coherences between all vibrational states. The relative amplitudes of multiquantum coherences are determined by the Taylor expansion of $\alpha(Q)$. In the WN approxi-

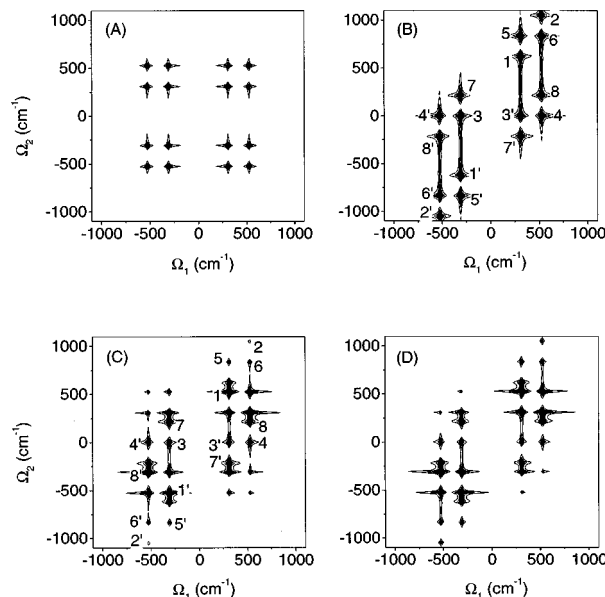


FIG. 6. 2D Raman spectrum $|S(\omega_2, \omega_1)/\tilde{\alpha}|$ of two coupled oscillators described by the Hamiltonian Eq. (C1) with vibrational frequencies $\Omega_1 = 311 \text{ cm}^{-1}$, and $\Omega_2 = 525 \text{ cm}^{-1}$, damping $\gamma_1 = \gamma_2 = 5 \text{ cm}^{-1}$ and anharmonicity $\tilde{V}_{nms}^{(3)} = 26 \text{ cm}^{-1}$, (for all $n, m, s = 1, 2$). Calculations were made using Eqs. (C6)–(C8), setting $\tilde{\alpha}_1^{(1)} = \tilde{\alpha}_2^{(1)}$, $\tilde{\alpha}_{1,1}^{(2)} = \tilde{\alpha}_{2,2}^{(2)} = \tilde{\alpha}_{1,2}^{(2)} = \tilde{\alpha}_{2,1}^{(2)} \tilde{\alpha}_1^{(1)}/\tilde{\alpha}_{1,1}^{(2)} = 10$, and defining $\tilde{\alpha} = (\tilde{\alpha}_1^{(1)})^2 \tilde{\alpha}_{1,1}^{(2)}$. The total signal has the following contributions: (A) $|S_1/\tilde{\alpha}|$ [Eq. (C6)] with resonances on oscillator vibrational frequencies $(\pm\Omega_1, \pm\Omega_2)$, and $(\mp\Omega_1, \pm\Omega_2)$, (B) $|S_2/\tilde{\alpha}|$ [Eq. (C7)] with overtones 1. $(\Omega_1, 2\Omega_1)$, 2. $(\Omega_2, 2\Omega_2)$, zero-frequency resonances 3. $(\Omega_1, 0)$, 4. $(\Omega_2, 0)$, and cross peaks 5. $(\Omega_1, \Omega_1 + \Omega_2)$, 6. $(\Omega_2, \Omega_1 + \Omega_2)$, 7. $(-\Omega_1, \Omega_2 - \Omega_1)$, 8. $(\Omega_2, \Omega_1 - \Omega_2)$ (resonances 1'–8' are related to 1–8 by inversion symmetry), and (C) $|S_3/\tilde{\alpha}|$ with the same resonances as in (A) (unmarked) and (B) (1–8, 1'–8'). In (A)–(B) intermode coupling originates from off-diagonal elements of the polarizability $\tilde{\alpha}_{nm}^{(2)}$ ($n \neq m$; $n, m = 1, 2$), whereas in (C) it originates from off-diagonal anharmonicities $\tilde{V}_{nms}^{(3)}$ ($n \neq m \neq s$; $n, m, s = 1, 2$). (D) The total signal $|S_1 + S_2 + S_3/\tilde{\alpha}|$ which contains all resonances shown in (A)–(C).

mation we truncate this expansion at $(Q/Q_0)^2$, constraining the excitations to the first three vibrational levels, resulting in a single echo at $t_1 = t_2$. In the HT ($g_T \gg 1$) limit all terms in the expansion of $\alpha(Q)$ contribute to the response, resulting in a multitude of echoes. Quantum effects which give additional echoes can be neglected when $g_h \ll 1$. The HT and WN both hold when $g_h \ll g_T \ll 1$.

For simplicity we have assumed in this paper an exponential form of $\alpha(Q)$ [Eq. (2.3)]. For this model the Gaussian form of the wave packets is maintained. The present results can however be used to compute the wave packets and response functions for an arbitrary dependence of $\alpha(Q)$. To that end we perform the Fourier transform

$$\alpha(Q) = \int_{-\infty}^{\infty} dk \tilde{\alpha}(k) \exp(ikQ), \quad (7.1)$$

$\alpha(Q)$ is then represented as a sum (or an integral) over exponentials.

Denoting the wave packet given by Eq. (2.7) by $\alpha_0 \rho^{(1)}(P, Q; 1/Q_0, \tau)$ (highlighting its parametric depen-

dence on Q_0), and making use of Eq. (7.1) we obtain for the wave packet $\rho^{(1)}(P, Q; \tau)$ which is related to an arbitrary form of the electronic polarization $\alpha(Q)$

$$\rho^{(1)}(P, Q; \tau) = \int_{-\infty}^{\infty} dk \tilde{\alpha}(k) \rho^{(1)}(P, Q; ik, \tau). \quad (7.2)$$

The third-order response function similarly adopts the form

$$R^{(3)}(t; \tau_1) = \int_{-\infty}^{\infty} dk \int_{-\infty}^{\infty} dP \int_{-\infty}^{\infty} dQ \tilde{\alpha}(k) \alpha(Q) \times \rho^{(1)}(P, Q; ik, \tau). \quad (7.3)$$

The present expressions for the wave packets (and response functions) can thus be used as *generating functions* for computing these quantities in the general case. The wave packet associated with each Liouville space pathway is given as a superposition of Gaussians throughout the propagation.

Finally we note that an extremely useful alternative algorithm for computing the quantum nonlinear response of high frequency modes is possible by using equations of motion for dynamical variables that include higher powers of Q and P , instead of the formal expansion in \hbar . The resulting nonlinear exciton equations (NEE) (Refs. 3,45–47) which have been developed and applied to models of coupled chromophores can then be effectively used to describe the nonlinear response of coupled vibrations.

ACKNOWLEDGMENTS

We gratefully acknowledge the support of the National Science Foundation and the United States Air Force Office of Scientific Research.

APPENDIX A: PHASE-MATCHING FOR IMPULSIVE PHOTON ECHOES

In this appendix we compute the impulsive photon echo signals in the WN limit [Eq. (3.2)]. We first consider a single harmonic mode with the spectral density,

$$C(\omega) = \frac{2\pi}{M\Omega} [\delta(\omega - \Omega) - \delta(\omega + \Omega)]. \quad (A1)$$

Substitution of Eq. (A1) into Eq. (2.19) gives

$$C(t) = -\frac{4\theta(t)}{M\Omega} \sin(\Omega t). \quad (A2)$$

To compute the optical response we substitute Eq. (A2) into Eq. (3.2) retaining only the second, echo-type, term. Further substitution of the resulting expression for $R^{(5)}(t_2, t_1)$ into Eq. (1.3) yields

$$P^{(5)}(t) = 4(\tilde{\alpha}^{(1)})^2 \alpha^{(2)} \int_{-\infty}^{\infty} d\tau'_1 \int_{-\infty}^{\infty} d\tau'_2 \times \sin \Omega(t - \tau'_2) \sin \Omega(\tau'_2 - \tau'_1) \times \mathcal{E}_2^2(\tau'_2 - \tau_2) \mathcal{E}_1^2(\tau'_1 - \tau_1) \mathcal{E}_p(t - t_p), \quad (A3)$$

where $\tilde{\alpha}^{(1)} = \alpha_0 / \sqrt{M\Omega Q_0}$ and $\tilde{\alpha}^{(2)} = \alpha_0 / (M\Omega Q_0)$.

We assume that each pair of pulses have the same temporal profile but different directions. The optical field is represented in the form

$$\mathcal{E}_j(t) = \frac{1}{2} E_j(t) e^{-i\omega_0 t} [e^{i\mathbf{k}'_j \cdot \mathbf{r}} + e^{i\mathbf{k}''_j \cdot \mathbf{r}}] + \text{c.c.} \quad (A4)$$

In Eq. (A4), \mathbf{k}' and \mathbf{k}'' are the two wave vectors of a pair, ω_0 is its optical frequency, \mathbf{r} is the position, $E_j(t)$ is a complex field representing the positive frequency part of the field.

The expression for the signal [Eq. (A3)] contains the square of the optical field. Neglecting terms which oscillate with the optical frequency yields

$$\mathcal{E}_j^2(t) = \frac{1}{2} |E_j(t)|^2 [1 + \cos(\Delta \mathbf{k}_j \cdot \mathbf{r})] \quad (A5)$$

with $\Delta \mathbf{k}_j \equiv \mathbf{k}'_j - \mathbf{k}''_j$. Taking the probe field $\mathcal{E}_p(t)$ in the form

$$\mathcal{E}_p(t) = \frac{1}{2} E_p(t) e^{-i\omega_0 t} e^{i\mathbf{k}_p \cdot \mathbf{r}} + \text{c.c.} \quad (A6)$$

and making use of the fact that the impulsive pulses are short compared to Ω^{-1} the polarization $P^{(5)}(t)$ in Eq. (A3) adopts the form

$$P^{(5)}(t) = e^{-i\omega_0(t-t_p)} E_p(t-t_p) \times \sum_{\mathbf{k}_s} \bar{P}(t_2, t_1; \mathbf{k}_s) e^{i\mathbf{k}_s \cdot \mathbf{r}} + \text{c.c.}, \quad (A7)$$

where the signal wave vector \mathbf{k}_s in the sum in the r.h.s. of Eq. (A7) assumes the values $\mathbf{k}_s = \mathbf{k}_p + m_1 \Delta \mathbf{k}_1 + m_2 \Delta \mathbf{k}_2$ with $m_1, m_2 = 0, \pm 1$ and

$$\bar{P}(t_2, t_1; \mathbf{k}_s) \equiv \frac{1}{2} (\tilde{\alpha}^{(1)})^2 \tilde{\alpha}^{(2)} a_{m_2 m_1} \sin(\Omega t_2) \times \sin(\Omega t_1) F_1 F_2, \quad (A8)$$

where $a_{mn} = 1/2^{|m|+|n|}$ and

$$F_j \equiv \int_{-\infty}^{\infty} |E_j(\tau)|^2 d\tau. \quad (A9)$$

Assuming a large number of molecules per cubic wavelength λ^3 , the polarization $\bar{P}(t_2, t_1; \mathbf{k}_s)$ determines the signal in the direction \mathbf{k}_s .

It is convenient to use the probe field as the local oscillator in heterodyne detection,

$$\mathcal{E}_h(t) = \frac{1}{2} e^{-i\omega_0(t-t_p)} E_p(t-t_p) + \text{c.c.} \quad (A10)$$

The heterodyne signal $S_h(t_2, t_1; \mathbf{k}_s)$ measured in the direction \mathbf{k}_s is given by

$$S_h(t_2, t_1; \mathbf{k}_s) \equiv \int_{-\infty}^{\infty} dt P^{(5)}(t; \mathbf{k}_s) \mathcal{E}_h(t) \quad (A11)$$

and can be computed by the substitution of Eqs. (A7) and (A10) into Eq. (A11) which yields the signal in the form of Eq. (5.8). [Equation (5.8) has been obtained in Sec. V using an alternative derivation scheme based on wave packet dynamics.] Averaging the signal [Eq. (5.8)] over the distribution function [Eq. (4.11)] yields for $t_1, t_2 \gg \Delta^{-1}$

$$S_i^{(5)}(t_2, t_1; \mathbf{k}_s) = \frac{1}{8} (\tilde{\alpha}^{(1)})^2 \tilde{\alpha}^{(2)} a_i(\mathbf{k}_s) \exp\left[-\frac{\Delta^2(t_2 - t_1)^2}{2}\right] \times \cos[\Omega_0(t_2 - t_1)] F_1 F_2 F_p. \quad (\text{A12})$$

Equation (A12) shows an echo signal at $t_2 = t_1$ with the width Δ^{-1} . The echo signal which includes an Ω_0 oscillation, shows up in all nine possible directions $\mathbf{k}_s = \mathbf{k}_p + m_1 \Delta \mathbf{k}_1 + m_2 \Delta \mathbf{k}_2$ with relative intensity given by the factors $a_i(\mathbf{k}_s)$,

$$a_i(\mathbf{k}_s) = \sum_{m,n=0,\pm 1} \frac{(2\pi)^3}{2^{|n|+|m|}} \delta(\mathbf{k}_p + m\Delta\mathbf{k}_1 + n\Delta\mathbf{k}_2 - \mathbf{k}_s). \quad (\text{A13})$$

The dependence of the signal on the pulse envelopes is given by Eq. (A9).

APPENDIX B: PHASE-MATCHING FOR SEMI-IMPULSIVE PHOTON ECHOES

We first represent the signal in the form

$$S_{si}^{(5)}(t_2, t_1; \mathbf{k}_s) = \text{Re} \int_{-\infty}^{\infty} d\Omega W(\Omega) \int d\mathbf{r} e^{-i\mathbf{k}_s \cdot \mathbf{r}} \times \int_{-\infty}^{\infty} dt P^{(5)}(t, \mathbf{r}; \Omega) \mathcal{E}_h(t - t_p), \quad (\text{B1})$$

where t_2 and t_1 are the time delays between pulses, \mathbf{k}_s is the signal wave vector and $P^{(5)}$ is given by Eq. (A3). Substituting Eq. (A3) into Eq. (B1) and making a simple transformation of the time integration-variables yields

$$S_{si}^{(5)}(t_2, t_1; \mathbf{k}_s) = 4(\tilde{\alpha}^{(1)})^2 \tilde{\alpha}^{(2)} \text{Re} \int_{-\infty}^{\infty} d\Omega W(\Omega) \int d\mathbf{r} e^{i\mathbf{k}_s \cdot \mathbf{r}} \times \int_{-\infty}^{\infty} d\tau'_1 \int_{-\infty}^{\infty} d\tau'_2 \int_{-\infty}^{\infty} d\tau' \times \sin[\Omega t_2 + \Omega(\tau' - \tau'_2)] \times \sin[\Omega t_1 + \Omega(\tau'_2 - \tau'_1)] \times \mathcal{E}_2^2(\tau'_2, \mathbf{r}) \mathcal{E}_1^2(\tau'_1, \mathbf{r}) \mathcal{E}_p(\tau', \mathbf{r}) \mathcal{E}_h(\tau'). \quad (\text{B2})$$

In the semi-impulsive regime the pulse durations τ_p satisfy the condition $\Omega^{-1} \ll \tau_p \ll \Delta^{-1}$. The excitation should be resonant with vibronic transitions. Since the excitation of vibronic levels is produced by the square of the optical field [see, e.g., Eq. (A3)] this can be accomplished using pairs of pulses whose carrier frequency difference is tuned to be resonant with the vibrational transitions. The optical fields $\mathcal{E}_j(\tau, \mathbf{r})$, $j=1,2$ in the exciting pulses is thus taken in the form

$$\mathcal{E}_j(\tau, \mathbf{r}) = \frac{1}{2} [E'_j(\tau) e^{i\mathbf{k}'_j \cdot \mathbf{r} - i\omega_0 \tau} + E''_j(\tau) e^{i\mathbf{k}''_j \cdot \mathbf{r} - i(\omega_0 + j\Omega_0) \tau}] + \text{c.c.} \quad (\text{B3})$$

It is clearly seen from Eq. (B3) that the first pulse is resonant with the single-excitation vibronic transition whereas the second pulse produces a double excitation. The probe and heterodyne pulses have the form

$$\mathcal{E}_p(\tau, \mathbf{r}) = \frac{1}{2} E_p(\tau) e^{i\mathbf{k}_p \cdot \mathbf{r} - i\omega_0 \tau} + \text{c.c.}, \quad (\text{B4})$$

$$\mathcal{E}_h(\tau) = \frac{1}{2} E_h(\tau) e^{-i(\omega_0 + \Omega_0) \tau} + \text{c.c.}$$

The reason for the choice of the frequency differences in Eqs. (B3) and (B4) is as follows: to get an echo, the first pulse should produce a single excitation in the right component of the density matrix whereas the second pulse should create a double excitation in the left component, which yields the frequency shifts of Ω_0 and $2\Omega_0$ respectively, in Eq. (B3). The polarization is induced by the matrix element between the singly and doubly-excited levels. This implies that the signal frequency is shifted by Ω_0 with respect to the probe, and the heterodyne frequency should be equal to $\omega_0 + \Omega_0$.

Neglecting terms which oscillate at optical frequencies we have

$$\mathcal{E}_m^2(\tau, \mathbf{r}) = \frac{1}{4} E''_m(\tau) E'_m{}^*(\tau) e^{-im\Omega_0 \tau + i\mathbf{k}_m \cdot \mathbf{r}} + \text{c.c.}, \quad (\text{B5})$$

with $m=1,2$ and $\Delta \mathbf{k}_m \equiv \mathbf{k}''_m - \mathbf{k}'_m$ and

$$\mathcal{E}_p(\tau, \mathbf{r}) \mathcal{E}_h(\tau) = \frac{1}{4} E_h(\tau) E_p^*(\tau) e^{-i\Omega_0 \tau - i\mathbf{k}_p \cdot \mathbf{r}}. \quad (\text{B6})$$

In Eq. (B5) we have also omitted the terms which do not oscillate with vibrational frequencies since they do not contribute to the echo. To derive the final expression for the signal, we first substitute Eqs. (B5) and (B6) into Eq. (B2), represent the sines in Eq. (B2) as linear combinations of exponents, and retain only the echo-contributing terms, i.e., those which contain $\exp[\pm i\Omega(t_2 - t_1)]$. We then integrate over τ'_1, τ'_2 , and τ' applying the rotating wave approximation, i.e., neglecting integrands oscillating with vibrational frequencies and making use of the fact that the pulses are much shorter than Ω^{-1} . These integrations yield the factor $\mathcal{F}_1^* \mathcal{F}_2 \mathcal{F}_p$ where

$$\mathcal{F}_m \equiv \int_{-\infty}^{\infty} d\tau E''_m(\tau) E'_m{}^*(\tau) \quad m=1,2, \quad (\text{B7})$$

$$\mathcal{F}_p \equiv \int_{-\infty}^{\infty} d\tau E_p(\tau) E_h^*(\tau).$$

Further integration over \mathbf{r} in Eq. (B2) yields a signal in the form of Eq. (5.13) with the spatial phase-matching factor $a_{si}(\mathbf{k}_s) \equiv (2\pi)^3 \delta[\mathbf{k}_s - (\mathbf{k}_p + \Delta \mathbf{k}_2 - \Delta \mathbf{k}_1)]$. Integrating over Ω using Eq. (4.11) we finally obtain for the semi-impulsive echo signal

$$S_{si}^{(5)}(t_2, t_1; \mathbf{k}_s) = \frac{1}{128} a_{si}(\mathbf{k}_s) (\tilde{\alpha}^{(1)})^2 \tilde{\alpha}^{(2)} \times \exp\left[-\frac{\Delta^2(t_2 - t_1)^2}{2}\right] \times \text{Re}(\mathcal{F}_1^* \mathcal{F}_2 \mathcal{F}_p). \quad (\text{B8})$$

Equation (B8) gives an echo at $t_2 = t_1$ in a single direction $\mathbf{k}_s = \mathbf{k}_p + \Delta \mathbf{k}_2 - \Delta \mathbf{k}_1$. Its magnitude is determined by Eqs. (B7), and in contrast to the impulsive regime the semi-impulsive echo does not show vibrational frequency oscillations.

APPENDIX C: FREQUENCY-DOMAIN WEAK-NONLINEARITY RESPONSE OF A MULTIMODE ANHARMONIC OSCILLATOR SYSTEM

We consider a molecular system with N primary Raman-active vibrational coordinates $\{Q_j\}$ ($j=1, \dots, N$), coupled to the optical field and interacting with harmonic bath coordinates. The Hamiltonian has the form of Eq. (2.1), where the molecular Hamiltonian is

$$H_m = \sum_{j=1}^N \left(\frac{P_j^2}{2M_j} + \frac{M_j \Omega_j^2 Q_j^2}{2} \right) + V(\mathbf{Q}), \quad (\text{C1})$$

with conjugated momenta P_j , harmonic oscillator frequencies Ω_j , and masses M_j . Anharmonicity of the nuclear potential energy is introduced by $V(\mathbf{Q})$ which can be expanded in the power series

$$V(\mathbf{Q}) = \sum_{k=3}^{\infty} \sum_{j_1, \dots, j_k=1}^N \frac{1}{k!} V_{j_1, \dots, j_k}^{(k)} Q^{j_1} \dots Q^{j_k}. \quad (\text{C2})$$

Coupling to the electric field is given by Eq. (1.1) in which the electronic polarizability depends on the primary oscillator coordinates \mathbf{Q} and can be represented by the expansion

$$\alpha(\mathbf{Q}) = \sum_{k=2}^{\infty} \sum_{j_1, \dots, j_k=1}^N \frac{1}{k!} \alpha_{j_1, \dots, j_k}^{(k)} Q^{j_1} \dots Q^{j_k}. \quad (\text{C3})$$

In the WN approximation we retain only first terms [$k=3$ in Eq. (C2) and $k=2$ in Eq. (C3)].

The response function $R^{(5)}(t_2+t_1; t_1; 0)$ in the WN approximations has three contributions

$$R^{(5)}(t_2+t_1; t_1; 0) = \sum_{\alpha=1}^3 R_{\alpha}^{(5)}(t_2+t_1; t_1; 0). \quad (\text{C4})$$

Expressions for all $R_{\alpha}^{(5)}$ were given in Ref. 28. We adopt the multi-mode underdamped Brownian oscillator model described by the Hamiltonian

$$H_B = \sum_{j, \alpha} \left[\frac{P_{\alpha}^2}{2m_{\alpha}} + \frac{m_{\alpha} \omega_{\alpha}^2}{2} \left(q_{\alpha} - \frac{c_{j\alpha}}{m_{\alpha} \omega_{\alpha}} Q_j \right)^2 \right], \quad (\text{C5})$$

with $c_{j\alpha}$ being the coupling constant between the primary oscillator and bath coordinates. The signal in the frequency domain [Eq. (6.1)], for underdamped oscillators is given by a sum of three contributions

$$S_1(\omega_2, \omega_1) = 16 \sum_{mn} \tilde{\alpha}_m^{(1)} \tilde{\alpha}_n^{(1)} \tilde{\alpha}_{mn}^{(2)} \times \frac{\Omega_m \Omega_n}{[(\omega_1 + i\gamma_m)^2 - \Omega_m^2][(\omega_2 + i\gamma_n)^2 - \Omega_n^2]}, \quad (\text{C6})$$

$$S_2(\omega_2, \omega_1) = 8 \sum_{mn} \tilde{\alpha}_m^{(1)} \tilde{\alpha}_n^{(1)} \tilde{\alpha}_{mn}^{(2)} \frac{1}{(\omega_1 + i\gamma_m)^2 - \Omega_m^2} \times \left\{ \frac{(\omega_1 + i\gamma_m)[\omega_2 + i(\gamma_m + \gamma_n)] + \Omega_m(\Omega_m - \Omega_n)}{[\omega_2 + i(\gamma_m + \gamma_n)]^2 - (\Omega_m - \Omega_n)^2} - \frac{(\omega_1 + i\gamma_m)[\omega_2 + i(\gamma_m + \gamma_n)] + \Omega_m(\Omega_m + \Omega_n)}{[\omega_2 + i(\gamma_m + \gamma_n)]^2 - (\Omega_m + \Omega_n)^2} \right\}, \quad (\text{C7})$$

$$S_3(\omega_2, \omega_1) = -32 \sum_{mns} \tilde{V}_{mns}^{(3)} \tilde{\alpha}_m^{(1)} \tilde{\alpha}_n^{(1)} \tilde{\alpha}_s^{(1)} \frac{\Omega_s}{(\omega_2 + i\gamma_s)^2 - \Omega_s^2} \times \left\{ \frac{1}{\omega_1 + i\gamma_m - \Omega_m} \frac{\Omega_n}{[\omega_2 + i(\gamma_m + \gamma_n) - \Omega_m]^2 - \Omega_n^2} - \frac{1}{\omega_1 + i\gamma_m + \Omega_m} \frac{\Omega_n}{[\omega_2 + i(\gamma_m + \gamma_n) + \Omega_m]^2 - \Omega_n^2} \right\}, \quad (\text{C8})$$

where $n, m, s = 1, \dots, N$. The coefficients in Eqs. (C6)–(C8) are $\tilde{\alpha}_n^{(1)} = \alpha_n^{(1)}/(M_n \Omega_n)^{1/2}$, $\tilde{\alpha}_{n,m}^{(2)} = \alpha_{n,m}^{(2)}/(M_n M_m \Omega_n \Omega_m)^{1/2}$, $\tilde{V}_{mns}^{(3)} = V_{mns}^{(3)}/(M_m M_n M_s \Omega_m \Omega_n \Omega_s)^{1/2}$. These expressions are used in Fig. 6.

- ¹R. F. Loring and S. Mukamel, J. Chem. Phys. **83**, 2119 (1985); S. Mukamel and R. F. Loring, J. Opt. Soc. Am. B **3**, 595 (1986).
- ²Y. Tanimura and S. Mukamel, J. Chem. Phys. **99**, 9496 (1993).
- ³S. Mukamel, *Principles of Nonlinear Optical Spectroscopy* (Oxford University Press, New York, 1995).
- ⁴A. Laubereau and W. Kaiser, Rev. Mod. Phys. **50**, 607 (1978).
- ⁵R. Inaba, H. Okamoto, K. Yoshihara, and M. Tasumi, J. Phys. Chem. **97**, 7815 (1993).
- ⁶F. Libenberger, C. Rauscher, H.-G. Purucker, and A. Laubereau, J. Raman Spectrosc. **26**, 835 (1995).
- ⁷T. Joo and A. C. Albrecht, J. Chem. Phys. **99**, 3244 (1995).
- ⁸K. A. Nelson and E. P. Ippen, Adv. Chem. Phys. **75**, 1 (1989).
- ⁹W. P. de Boeij, M. S. Pshenichnikov, and D. A. Wiersma, J. Phys. Chem. **100**, 11806 (1996).
- ¹⁰K. D. Rektor, A. S. Kwok, C. Ferrante, A. Tokmakoff, C. W. Rella, and M. D. Fayer, J. Chem. Phys. **106**, 10027 (1997); L. R. Narasimhan, K. A. Littau, D. W. Pack, Y. S. Bai, Eischner, and M. D. Fayer, Chem. Rev. **90**, 439 (1990).
- ¹¹T. Joo, Y. W. Jia, J. Y. Yu, D. M. Jonas, and G. R. Fleming, J. Phys. Chem. **100**, 2399 (1996).
- ¹²R. Jankowiak and G. J. Small, Phys. Rev. B **47**, 14805 (1993).
- ¹³D. V. Bout, L. J. Muller, and M. Berg, Phys. Rev. Lett. **67**, 3700 (1991); M. Berg and D. A. V. Bout, Acc. Chem. Res. **30**, 65 (1997).
- ¹⁴R. Inaba, K. Tominaga, K. Tasumi, and M. Nelson, Chem. Phys. Lett. **211**, 183 (1993); K. Tominaga, R. Inaba, T. J. Kang, Y. Naitoh, K. A. Nelson, M. Tasumi, and K. Yoshihara, in *Proceedings of the Raman XIV International Conference on Raman Spectroscopy* (Wiley, New York, 1994); K. Yoshihara, R. Inaba, H. Okamoto, M. Tasumi, K. Tominaga, and K. A. Nelson, in *Femtosecond Reaction Dynamics*, edited by D. Wiersma (North-Holland, Amsterdam, 1994).
- ¹⁵V. Khidekel and S. Mukamel, Chem. Phys. Lett. **240**, 304 (1995); **263**, 350 (1996).
- ¹⁶A. Tokmakoff, M. J. Lang, D. S. Larsen, G. R. Fleming, V. Chernyak, and S. Mukamel, Phys. Rev. Lett. **79**, 14 (1997); **79**, 2702 (1997).
- ¹⁷T. Steffen and K. Duppen, Phys. Rev. Lett. **76**, 1224 (1996); J. Chem. Phys. **106**, 3854 (1997).

- ¹⁸T. Steffen, J. T. Fourkas, and K. Duppen, *J. Chem. Phys.* **105**, 7364 (1996).
- ¹⁹K. Tominaga and K. Yoshihara, *Phys. Rev. Lett.* **74**, 3061 (1995); K. Tominaga, G. P. Keogh, Y. Naitoh, and K. Yoshihara, *J. Raman Spectrosc.* **26**, 495 (1995); K. Tominaga, and K. Yoshihara, *J. Chem. Phys.* **104**, 1159 (1996); **104**, 4419 (1996); *Phys. Rev. Lett.* **76**, 987 (1996); *Phys. Rev. A* **55**, 831 (1997).
- ²⁰A. Tokmakoff and G. R. Fleming, *J. Chem. Phys.* **106**, 2569 (1997); A. Tokmakoff, M. J. Lang, D. S. Larsen, and G. R. Fleming, *Chem. Phys. Lett.* **272**, 48 (1997).
- ²¹A. Tokmakoff, *J. Chem. Phys.* **105**, 13 (1996).
- ²²K. Okumura and Y. Tanimura, *Chem. Phys. Lett.* **278**, 175 (1997); M. Cho, K. Okumura, and Y. Tanimura, *J. Chem. Phys.* **108**, 1326 (1998).
- ²³S. Mukamel, A. Piryatinski, and V. Chernyak, *Acc. Chem. Res.* (in press).
- ²⁴S. P. Palese, J. T. Buontempo, L. Schilling, W. T. Lotshaw, Y. Tanimura, S. Mukamel, and R. J. D. Miller, *J. Phys. Chem.* **98**, 12466 (1994).
- ²⁵K. Okumura and Y. Tanimura, *Phys. Rev. E* **53**, 214 (1996); *J. Chem. Phys.* **105**, 7294 (1996); **106**, 1687 (1997).
- ²⁶K. Okumura and Y. Tanimura, *Chem. Phys. Lett.* **277**, 159 (1997).
- ²⁷S. Saito and I. Ohmine, *J. Chem. Phys.* **108**, 240 (1998).
- ²⁸V. Chernyak and S. Mukamel, *J. Chem. Phys.* **108**, 5812 (1998).
- ²⁹R. W. Hellwarth, *Prog. Quantum Electron.* **5**, 2 (1997).
- ³⁰Strictly speaking, Eq. (1.4) has eight terms. However, the two terms obtained by the action of α_L and α_R of α_+ are identical. This cuts the number of terms by half.
- ³¹W. H. Miller, *Adv. Chem. Phys.* **25**, 69 (1974); *J. Chem. Phys.* **53**, 1949 (1970); **53**, 3578 (1970).
- ³²E. J. Heller, *J. Chem. Phys.* **65**, 4979 (1976).
- ³³M. Brach and R. K. Bhadur, *Semiclassical Physics* (Addison-Wesley, New York, 1997).
- ³⁴S. Mukamel, V. Khidekel, and V. Chernyak, *Phys. Rev. E* **53**, 1 (1996).
- ³⁵V. Khidekel, V. Chernyak, and S. Mukamel, *Femtochemistry*, edited by M. Chergui (World Scientific, Singapore, 1996), p. 507.
- ³⁶Y. Tanimura and S. Mukamel, *J. Opt. Soc. Am. B* **10**, 2263 (1993).
- ³⁷Y. J. Yan and S. Mukamel, *J. Chem. Phys.* **88**, 5735 (1988).
- ³⁸E. L. Hahn, *Phys. Rev.* **80**, 583 (1950).
- ³⁹J. K. M. Sanders and B. H. Hunter, *Modern NMR Spectroscopy* (Oxford, New York, 1993); R. R. Ernst, G. Bodenhausen, and A. Wokaun, *Principles of Nuclear Magnetic Resonance in One and Two Dimensions* (Clarendon, Oxford, 1987).
- ⁴⁰This initial condition represents the density matrix immediately after the first interaction with the field, i.e., $\hat{\alpha}_- \bar{\rho}(P, Q)$.
- ⁴¹A. O. Calderia and A. J. Leggett, *Physica A* **121**, 587 (1983).
- ⁴²D. Kohen and D. J. Tannor, *J. Chem. Phys.* **107**, 5141 (1997).
- ⁴³*Selected Papers on Noise and Stochastic Processes*, edited by N. Wax (Dover, New York, 1954).
- ⁴⁴V. Chernyak, A. Piryatinski, and S. Mukamel, *Laser Chem.* (in press).
- ⁴⁵V. Chernyak, W. M. Zhang, and S. Mukamel, *J. Chem. Phys.* **109**, 9587 (1998).
- ⁴⁶W. M. Zhang, V. Chernyak, and S. Mukamel, *J. Chem. Phys.* (submitted).
- ⁴⁷W. M. Zhang, V. Chernyak, and S. Mukamel, in *Proceedings of the XI International Conference on Ultrafast Phenomena* (Springer, Berlin, 1998); S. Mukamel, W. M. Zhang, and V. Chernyak, in *Proceedings of the XIth International Congress on Photosynthesis*, edited by G. Grab and J. Puztai (Kluwer Dordrecht, The Netherlands, 1998).